Brush border Myosin Ia has tumor suppressor activity in the intestine

Rocco Mazzolini[a,b], Higinio Dopeso[a,b,1], Silvia Mateo-Lozano[a,b,1], Wakam Chang[c], Paulo Rodrigues[a,b], Sarah Bazzocco[a], Hafid Alazzouzi[a], Stefania Landolfi[d], Javier Hernández-Losa[d], Elena Andretta[a,b], Pia Alhopuro[e], Eloy Espín[f], Manel Armengol[f], Josep Tabernero[g], Santiago Ramón y Cajal[d], Matthias Kloor[h], Johannes Gebert[h], John M. Mariadason[i], Simo Schwartz, Jr.[b,j], Lauri A. Aaltonen[e], Mark S. Mooseker[c], and Diego Arango[a,b,2]

[a]Group of Molecular Oncology, and [j]Group of Drug Delivery and Targeting, Centro de Investigaciones en Bioquímica y Biología Molecular-Nanomedicine, Vall d'Hebron University Hospital Research Institute, Universitat Autònoma de Barcelona, 08035 Barcelona, Spain; [b]Centro de Investigación Biomédica en Red de Bioingeniería, Biomateriales y Nanomedicina, 50018 Zaragoza, Spain; [c]Department of Molecular, Cellular, and Developmental Biology, Yale University, New Haven, 06520-8103 CT; [d]Department of Pathology, [f]Department of Surgery, and [g]Department of Medical Oncology, Vall d'Hebron University Hospital, Universitat Autònoma de Barcelona, 08035 Barcelona, Spain; [e]Department of Medical Genetics, Genome-Scale Biology Research Program, Biomedicum Helsinki, University of Helsinki, 00014 Helsinki, Finland; [h]Department of Applied Tumor Biology, Institute of Pathology, University Hospital Heidelberg, 69120 Heidelberg, Germany; and [i]Ludwig Institute for Cancer Research, Melbourne Centre for Clinical Sciences, Austin Health, Heidelberg, Victoria 3084, Australia

Edited* by Albert de la Chapelle, Ohio State University Comprehensive Cancer Center, Columbus, OH, and approved December 20, 2011 (received for review June 3, 2011)

The loss of the epithelial architecture and cell polarity/differentiation is known to be important during the tumorigenic process. Here we demonstrate that the brush border protein Myosin Ia (MYO1A) is important for polarization and differentiation of colon cancer cells and is frequently inactivated in colorectal tumors by genetic and epigenetic mechanisms. *MYO1A* frame-shift mutations were observed in 32% (37 of 116) of the colorectal tumors with microsatellite instability analyzed, and evidence of promoter methylation was observed in a significant proportion of colon cancer cell lines and primary colorectal tumors. The loss of polarization/differentiation resulting from MYO1A inactivation is associated with higher tumor growth in soft agar and in a xenograft model. In addition, the progression of genetically and carcinogen-initiated intestinal tumors was significantly accelerated in *Myo1a* knockout mice compared with *Myo1a* wild-type animals. Moreover, MYO1A tumor expression was found to be an independent prognostic factor for colorectal cancer patients. Patients with low MYO1A tumor protein levels had significantly shorter disease-free and overall survival compared with patients with high tumoral MYO1A (logrank test $P = 0.004$ and $P = 0.009$, respectively). The median time-to-disease recurrence in patients with low MYO1A was 1 y, compared with >9 y in the group of patients with high MYO1A. These results identify MYO1A as a unique tumor-suppressor gene in colorectal cancer and demonstrate that the loss of structural brush border proteins involved in cell polarity are important for tumor development.

Loss of cell polarity, differentiation, and tissue architecture are hallmarks of advanced metastatic carcinomas and strongly correlate with poor patient prognosis (1). The mechanisms regulating this epithelial-to-mesenchymal transition are well characterized (2). However, the importance of the loss of cell polarity and differentiation during premetastatic epithelial tumorigenesis is not well understood. Recent evidence from model organisms indicates that genes regulating cell polarity and differentiation in epithelial cells can have tumor-suppressor activity, although the role of polarity regulators in human cancer has not been thoroughly investigated (1, 3, 4). The Ser/Thr kinase 11 (STK11; also known as LKB1) regulates cellular metabolism and proliferation and has recently been shown to be a master regulator of polarity in epithelial cells (5, 6). Germ-line *STK11/LKB1* mutations are responsible for Peutz-Jeghers syndrome, an autosomal dominant genetic disease characterized by the development of benign hamartomatous intestinal polyps and predisposition to different types of cancer, including colorectal cancer (7–9). Importantly, the suppressor activity of STK11/LKB1 in intestinal epithelial cells seems to be associated with the regulation of cell polarity and differentiation rather than its role in cell cycle and metabolic control (10). However, *STK11/LKB1* mutations are rare in sporadic colorectal tumors and epigenetic inactivation is not frequently observed (11–13), suggesting that alternative genetic/epigenetic mechanisms exist in intestinal tumor cells to disrupt epithelial cell polarity and differentiation during the earlier stages of the tumorigenic process.

The intestinal epithelium is among the most rapidly proliferating tissues in the human adult body. This cell monolayer lining the inner surface of the intestine is in constant renewal, with cells rapidly proliferating in the lower part of the intestinal crypts of Lieberkuhn. These immature cells migrate toward the top of the crypts and into the villi of the small intestine or the flat colonic mucosa as they differentiate, and are eventually shed into the intestinal lumen (14). The stem cells of the system are located in the bottom of the crypts (15, 16) and give rise to all of the cell types of this epithelium, namely, absorptive, goblet, enteroendocrine, and Paneth cells. Differentiated intestinal epithelial cells are highly polarized with a well-defined apical and basolateral domain. Differentiated cells of the absorptive lineage show a characteristic apical brush border consisting of a tight array of microvilli that significantly increase the contact surface with the intestinal contents. The core of each microvillus is maintained by a dense bundle of actin filaments cross-linked by fimbrin, villin, and espin. Myosin Ia (MYO1A) is a major component of the cytoskeleton that underlies and supports the apical brush border of the enterocytes (17). MYO1A forms a spiral array of bridges that links the microvillar actin core to the membrane (18–20). The loss of structural proteins supporting the complex cytoskeleton of the brush border is generally believed to be the result of the de-differentiation and loss of polarization occurring during tumor progression. A causative role for these proteins in the tumorigenic process has never been observed. Here we show that the gene encoding Myosin Ia (*MYO1A*) regulates the polarization/differentiation of colorectal cancer cells, is frequently mutated/methylated in colorectal tumors, and has tumor-suppressor activity.

Author contributions: D.A. designed research; R.M., H.D., S.M.-L., W.C., P.R., S.B., H.A., E.A., J.G., J.M.M., and D.A. performed research; R.M., H.D., S.M.-L., W.C., P.R., S.B., H.A., S.L., J.H.-L., P.A., E.E., J.T., M.A., S.R.y.C., M.K., J.G., J.M.M., S.S., L.A.A., M.S.M., and D.A. contributed new reagents/analytic tools; R.M., H.D., S.M.-L., W.C., P.R., S.B., H.A., S.L., P.A., M.K., J.G., J.M.M., L.A.A., M.S.M., and D.A. analyzed data; and R.M. and D.A. wrote the paper.

The authors declare no conflict of interest.

*This Direct Submission article had a prearranged editor.

[1]H.D. and S.M.-L. contributed equally to this work.

[2]To whom correspondence should be addressed. E-mail: diego.arango@vhir.org.

This article contains supporting information online at www.pnas.org/lookup/suppl/doi:10.1073/pnas.1108411109/-/DCSupplemental.

Results

Frequent MYO1A Mutations in Colorectal Tumors with Microsatellite Instability. A subset of colorectal tumors accumulates mutations mainly in microsatellite repeats throughout the genome because of defects in mismatch repair mechanisms. Frame-shift mutations in coding microsatellites of tumor-suppressor genes may confer a growth advantage to cancer cells and are therefore observed at high frequency in colorectal tumors with microsatellite instability (MSI). We found frame-shift mutations in an A8 microsatellite repeat located in the last exon (Ex 28) of *MYO1A* in 44.4% (16 of 36) and 31.3% (42 of 134) of MSI colorectal cancer cell lines and primary tumors, respectively (*SI Appendix*, Fig. S1 *A* and *B*, and Tables S1 and S2). No mutations were observed in the matching normal DNA of these cases. As a control, a noncoding A8 microsatellite in intron 22–23, located 4.7-Kb upstream of the coding A8 in exon 28, showed no mutations in a subset of 23 MSI primary colorectal tumors and 11 MSI lines studied (Fisher's exact test, $P < 0.0001$). Moreover, the frequency of mutations in *MYO1A* observed was above the 95% prediction interval expected for A8 repeats when plotted against the mutation frequency in a series of 62 intronic A/T repeats in MSI colorectal tumors (*SI Appendix*, Fig. S1*C*), collectively suggesting that the mutations observed in *MYO1A* are clonally selected and confer a growth advantage to these tumors. The full *MYO1A* coding region of seven MSI colorectal cancer lines with heterozygous mutations in the A8 tract in Exon 28 was sequenced, and no additional mutations were found. To further investigate the role of *MYO1A* mutations in tumor progression, we also sequenced this region in 17 MSI adenomas and found 2 A8→A7 mutations (11.8%). A significant association was observed between mutation frequency and tumor stage (*SI Appendix*, Fig. S1*D*). *MYO1A* was mutated in 19% of the premalignant lesions (adenomas) and tumors that have not invaded through the intestinal wall (Dukes A) compared with 35% of the tumors that had invaded through the gut wall or metastasized to regional lymph nodes or distant organs (Dukes B–D; Fisher's exact test, $P = 0.04$), suggesting that *MYO1A* inactivation is important for local tumor invasion through the intestinal wall but does not confer an increased metastatic potential.

Fifty-five of the 58 mutations (95%) observed in the tumor lines and primary colorectal tumors studied were deletions of one A in the A8 repeat in exon 28 of *MYO1A* (MYO1A^{A7MUT}) (*SI Appendix*, Fig. S1*A*). This mutation causes a frame-shift and a premature stop codon and, as a result, the last 11 amino acids of the wild-type MYO1A are replaced by 7 different amino acids (*SI Appendix*, Fig. S2*A*). Previous studies have shown that the tail domain of MYO1A is necessary and sufficient for localization to the plasma membrane (21, 22). To investigate the effects of the observed *MYO1A* mutations on its function and subcellular localization, wild-type or mutant full-length MYO1A and MYO1A tail domain were transfected into Caco2 colon cancer cells and the derivative clone Caco2$_{BBe}$. Transfection of the full-length wild-type EGFP-MYO1A protein and the wild-type EGFP-tail domain (*SI Appendix*, Fig. S2*B*) showed membrane localization in both undifferentiated (Fig. 1*A*) and fully differentiated Caco2 cells (Fig. 1*E*). In contrast, the EGFP/ERFP-tagged full-length MYO1A^{A7MUT} and tail^{A7MUT} domain mutant proteins failed to localize to the membrane and were instead mislocalized to the cytoplasm in both undifferentiated and differentiated Caco2 cells (Fig. 1 *B* and *H*), demonstrating that the frequently observed MYO1A^{A7} mutations interfere with the subcellular localization of MYO1A.

Promoter Methylation Regulates MYO1A Expression. Although no mutations were found in the coding region of 10 microsatellite stable (MSS) colon cancer cell lines, we found frequent promoter hypermethylation in both MSI and MSS colon cancer cell lines. Despite the absence of a dense CpG island in the *MYO1A* promoter (*SI Appendix*, Fig. S3), quantitative assessment of the levels of methylation in two CpG dinucleotides located −154 bp and +271 bp relative to the transcription start site revealed

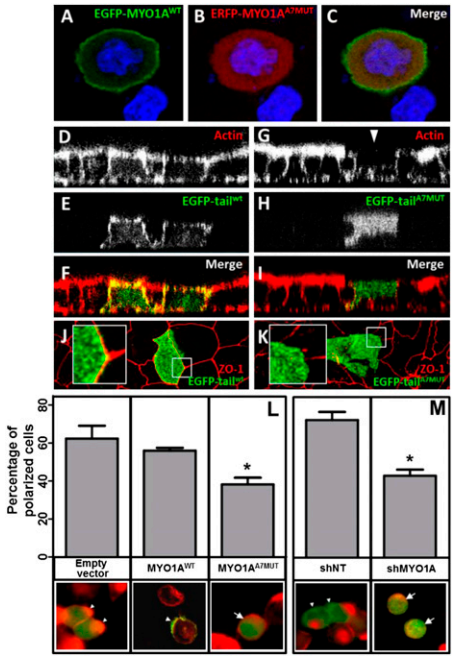

Fig. 1. MYO1A A8->A7 mutations affect the localization of the protein and the polarization of colon cancer cells. (*A–C*) Cotransfection of wild-type EGFP-MYO1A^{wt} and mutant ERFP-MYO1A^{A7MUT} demonstrated that the mutant protein mislocalized to the cytoplasm of undifferentiated Caco2 cells. (*D–I*) An orthogonal view of differentiated Caco2$_{BBe}$ cells. Alexa 568-labeled Phalloidin was used to visualize F-actin. Wild-type MYO1A EGFP-tail^{wt} showed membrane localization (*D–F*) compared with the cytoplasmic localization of mutant MYO1A EGFP-tail^{A7MUT} (*G–I*). F-actin was reduced in the apical membrane of MYO1A EGFP-tail^{A7MUT}-expressing cells (*G*, white arrowhead). ZO-1 immunostaining demonstrated that MYO1A EGFP-tail^{A7MUT}–expressing Caco2$_{BBe}$ cells exhibit loss of tight junctional integrity (*z*-axis stack; *J–K*). (*Inset*) Higher magnification of the indicated areas demonstrating loss of ZO-1 membrane staining in EGFP-Tail^{A7MUT} transfected cells. Induction of LKB1/STK11 expression resulted in the polarization of most LS174T-W4 cells characterized by the apical accumulation of actin within 24 h (white arrowheads in *L* and *M*). The number of polarized cells 24 h after LKB1/STK11 activation was significantly reduced following transfection of either mutant EGFP-MYO1A^{A7MUT} (*L*, mean ± SE; Student's *t* test, $*P = 0.03$) or cotransfection of EGFP and shMYO1A (*M*; mean ± SE; Student's *t* test, $*P = 0.01$), compared with the corresponding pEGFP-C3 empty vector, EGFP-MYO1A^{WT} and nontarget shRNA (shNT) controls. Rhodamine-Phalloidin was used to visualize F-actin (red). White arrows show unpolarized transfected cells. The average (± SE) of three independent experiments is shown. Original magnification is 600×.

frequent methylation in a panel of 46 colorectal cancer cell lines (50% of the lines showed levels of methylation >50%) (*SI Appendix*, Fig. S3 and Table S2). Moreover, the levels of methylation in these two CpGs correlated positively with each other (Pearson's $r = 0.75$; $P < 0.0001$) (*SI Appendix*, Fig. S4*A*) and negatively with the levels of mRNA expression in these cell lines (Pearson's $r = -0.54$; $P = 0.005$) (*SI Appendix*, Fig. S4*B*). Although normal colonic mucosal samples typically contain high levels of contamination with nonepithelial cells, the average level of *MYO1A* promoter methylation at CpG −154 bp and +271 bp was significantly lower in normal colon samples compared with normal breast, stomach, ovary, lung, or kidney samples (Student's *t* test, $P < 2.6 \times 10^{-19}$) (*SI Appendix*, Fig. S4*C*). Analysis of a series of 122 primary colorrectal tumors demonstrated that the levels of methylation at these CpG dinucleotides were significantly correlated with the levels of MYO1A mRNA expression (Pearson's $r < -0.41$; $P < 0.0001$) (*SI Appendix*, Fig. S4 *D* and *E*). Methylation was confirmed by direct sequencing of bisulfite treated DNA in a subset of samples (*SI Appendix*, Fig. S3 and Table S2). The activity of cellular DNA methyltransferases was

reduced in cell lines with high *MYO1A* promoter methylation using either a pharmacologic (5-Aza-2′-deoxycytidine treatment in HCT116 and Co115 cells) or genetic approach (targeted deletion of the DNA methyltransferases *DNMT1* and *DNMT3b* in HCT116 cells) and resulted in a reduction in the levels of methylation in the *MYO1A* promoter (*SI Appendix*, Fig. S5 *A*, *C*, *E*, and *F*) that was associated with a significant increase in the levels of expression of MYO1A (*SI Appendix*, Fig. S5 *B*, *D*, and *G*). Collectively, these results demonstrate that *MYO1A* promoter methylation is a common event that regulates *MYO1A* expression in colorectal tumors.

MYO1A Regulates Differentiation and Polarization of Colon Cancer Cells. Because MYO1A is important for the apical localization of additional brush border proteins (22), we next assessed whether MYO1A can regulate cell polarity and differentiation of colon cancer cells. The apical accumulation of F-actin is a hallmark of epithelial differentiation along the absorptive cell lineage (5). Fully differentiated Caco2 cells, which express high levels of wild-type MYO1A protein (*SI Appendix*, Fig. S6*A*), when transfected with the mutant MYO1A EGFP-tail^{A7MUT} frequently failed to develop the characteristic accumulation of actin in the apical brush border (Fig. 1*G*). In addition, mutant EGFP-tail^{A7MUT}-expressing cells exhibit loss of tight junctional integrity as assessed by reduced levels of the junction-associated protein ZO-1 (Fig. 1 *J* and *K*). To further investigate the role of MYO1A in the polarization of colon cancer cells, we used an in vitro system where a fully polarized phenotype can be induced by constitutive overexpression of the pseudokinase STRAD and inducible expression of LKB1/STK11 in LS174T-W4 colon cancer cells (5) that express endogenous wild-type MYO1A (*SI Appendix*, Fig. S7 and Table S2). Transfection of either shMYO1A (which induced a 51% decrease in MYO1A protein expression) (*SI Appendix*, Fig. S8) or mutant EGFP-MYO1A^{A7MUT} into LS174T-W4 cells interfered with the polarization of these cells upon induction of LKB1/STK11, compared with the nontarget shRNA or empty vector/EGFP-MYO1A^{wt} controls, respectively (Fig. 1 *L* and *M*). Moreover, stable shRNA-mediated down-regulation of MYO1A in Caco2 cells (*SI Appendix*, Fig. S6*A*) resulted in significantly reduced activity of alkaline phosphatase, sucrose isomaltase, and dipeptidyl-peptidase 4, three markers of differentiation along the absorptive cell lineage (*SI Appendix*, Fig. S6 *B–D*). In addition, dome formation following 21 d of confluent culture, an additional marker of differentiation of Caco2 monolayers (23), was also significantly reduced in cells transduced with shMYO1A compared with parental and nontarget shRNA transduced Caco2 cells (*SI Appendix*, Fig. S6*E*). Moreover, although SW403 cells do not undergo significant differentiation under confluent culture conditions, shRNA-mediated MYO1A knockdown interfered with the capacity of these cells to differentiate after treatment with the short-chain fatty acid butyrate, a potent inducer of differentiation in colorectal cancer cells (*SI Appendix*, Fig. S9). Collectively, these experiments demonstrate that MYO1A regulates the polarization and differentiation of colon cancer cells.

MYO1A Inhibits Tumor Growth. To investigate the possible functional contribution of the loss of MYO1A to tumor progression, we next investigated whether MYO1A regulates the growth of colon cancer cells using Caco2 and SW403 cells stably expressing shMYOA. Knockdown of MYO1A in these two cell lines (Fig. 2 *A* and *D*) resulted in a significant increase in the number of colonies observed when cells were grown in soft-agar medium compared with either the parental cell line or the nontarget shRNA control (Fig. 2 *B* and *E*), demonstrating that reduced MYO1A levels significantly improved the anchorage-independent growth of colon cancer cells. Moreover, when these cell lines were grown as xenografts in immunocompromised mice, MYO1A knockdown sublines grew significantly faster than the nontarget shRNA control lines (Fig. 2 *C* and *F*), indicating that reduced MYO1A levels confer a growth advantage to colon cancer cells in vivo.

Loss of MYO1A Accelerates Tumor Progression. To further investigate the role of MYO1A on intestinal tumorigenesis, we used a mouse model where the first three exons of *Myo1a* have been replaced by a neo/ura selection cassette, resulting in the complete absence of Myo1a protein (24). Although *Myo1a* knockout (KO) mice show important structural and compositional defects in the brush border domain of the intestinal epithelium, inactivation of *Myo1a* alone is not sufficient to initiate intestinal tumorigenesis (24). We therefore used both a genetic (*Apc* mutations; Apc^{min} mouse model) and a pharmacological (azoxymethane, AOM) approach to initiate intestinal tumorigenesis in *Myo1a* KO mice. Using the genetic model of tumor initiation, we found that animals were born at Mendelian ratios (78/138/73 for $Myo1a^{+/+}$, $Myo1a^{+/-}$, and $Myo1a^{-/-}$, respectively) and the weight of the animals with different genotype at 153 or 214 d of age was not significantly different (Student's *t* test, $P > 0.1$). However, introduction of a heterozygous or homozygous deletion of *Myo1a* in mice bearing the Apc^{min} mutation resulted in a significant shortening of their lifespan (Fig. 3*A*). The median survival of the animals in the $Apc^{min/+};Myo1a^{+/+}$ group was 378 d, which was reduced to 329 d (13%; logrank test, $P = 0.02$) and 245 d (35%; logrank test, $P = 0.0003$) for the $Apc^{min/+};Myo1a^{+/-}$ and $Apc^{min/+};Myo1a^{-/-}$ groups, respectively. In good agreement, scoring of microscopically and macroscopically visible small intestinal tumors demonstrated a significantly higher number of tumors in $Apc^{min/+};Myo1a^{-/-}$ and $Apc^{min/+};Myo1a^{+/-}$ mice compared with $Apc^{min/+};Myo1a^{+/+}$ animals (Fig. 3*B*).

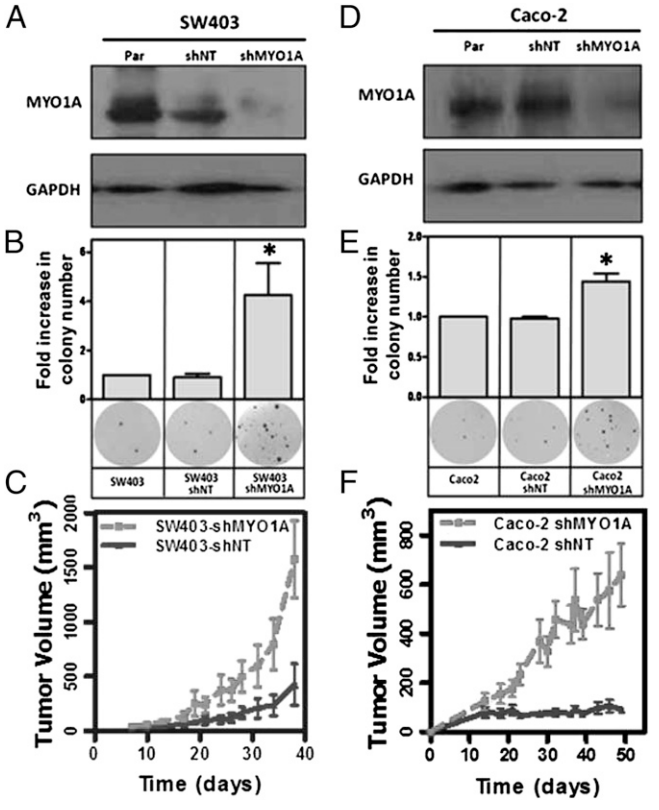

Fig. 2. MYO1A regulates the growth of colon cancer cells. Western blot analysis demonstrated that stable shRNA transduction resulted in reduced MYO1A levels in Caco2 and SW403 colon cancer cells (*A* and *D*) (Par, parental cells; shNT and shMYO1A, cells transduced with a nontarget shRNA or shMYO1A, respectively). MYO1A knockdown cells showed increased anchorage-independent growth in soft agar medium (*B* and *E*) (mean of three independent experiments run in triplicate; Student's *t* test $*P < 0.001$). A significantly faster growth of the shMYO1A SW403 (*C*) and shMYO1A Caco2 (*F*) cells was observed in a xenograft model compared with the corresponding nontarget shRNA sublines.

Although *Myo1a* inactivation did not affect the average tumor size, we found >twofold increase in the number of infiltrating adenocarcinomas in $Apc^{min/+}$;$Myo1a^{-/-}$ compared with $Apc^{min/+}$;$Myo1a^{+/+}$ animals (11.9% versus 5.6%, respectively; Student's *t* test, $P = 0.05$) (Fig. 3 *C–F* and *SI Appendix*, Fig. S10). Examination of the normal mucosa demonstrated no differences in the total number of cells per crypt/villus or the frequency of goblet, Paneth, or enteroendocrine cells between $Apc^{min/+}$;$Myo1a^{+/+}$ and $Apc^{min/+}$;$Myo1a^{-/-}$ mice (*SI Appendix*, Fig. S11). Similarly, no differences were observed in the number of proliferating cells either in the normal epithelium or intestinal tumors from $Apc^{min/+}$ mice that were $Myo1a^{+/+}$, or $Myo1a^{-/-}$ (*SI Appendix*, Fig. S12). As an alternative mechanism to initiate intestinal tumorigenesis we used AOM, an intestinal-specific chemical carcinogen. Consistent with findings made in the Apc^{min} model, we observed a significantly higher number of tumors in the small intestine of $Myo1a^{+/+}$ mice compared with $Myo1a^{+/+}$ animals (2.5 ± 1.3 vs. 0.8 ± 0.7 tumors per mouse, respectively; Student's *t* test; $P = 0.001$) (*SI Appendix*, Fig. S13). When taken together, these results demonstrate that inactivation of *Myo1a* is an important event contributing to intestinal tumor progression and may participate in the adenoma-to-carcinoma transition.

Low Levels of MYO1A Are Associated with Shorter Survival of Colorectal Cancer Patients. Because *Myo1a* inactivation accelerated the oncogenic process in mouse models of intestinal tumorigenesis, we next investigated the possible association between MYO1A tumor levels and prognosis of patients with colorectal cancer. For this purpose we assessed the tumor levels of MYO1A protein in a series of 155 colorectal cancer patients with locally advanced disease (Dukes C) using immunohistochemical staining of sections of a tissue microarray (Fig. 4 *A–F* and *SI Appendix*, Table S3). Patients with low MYO1A tumor protein levels had significantly shorter disease-free and overall survival compared with patients with high tumoral MYO1A (Fig. 4 *G* and *H* and *SI Appendix*, Fig. S14) (logrank test, $P = 0.004$ and $P = 0.009$, respectively). The median time-to-disease recurrence in Dukes C patients with low MYO1A was 1 y, compared with >9 y in the group of patients with high MYO1A. Multivariate analysis showed that MYO1A remained a good marker of prognosis of colorectal cancer patients (overall and disease-free survival, Cox regression, $P < 0.04$; covariates: patient age, sex, adjuvant treatment, tumor location, and grade). Twenty-one of the 155 tumors in the tissue microarray were MSI and MYO1A mutation data were available, allowing analysis of a possible association between $MYO1A^{7A}$ mutations and expression levels. A significant reduction in MYO1A protein levels was observed in MSI tumors with *MYO1A* mutations ($n = 13$) compared with MSI tumors without mutations ($n = 8$; average score 2.1 ± 0.9 vs. 3.1 ± 0.9, respectively; Student's *t* test, $P = 0.031$). However, no difference in MYO1A protein expression was observed in primary Dukes C tumors and matched lymph node metastases ($n = 16$; average score 2.5 ± 0.6 vs. 2.2 ± 0.8 respectively; Student's *t* test, $P = 0.24$).

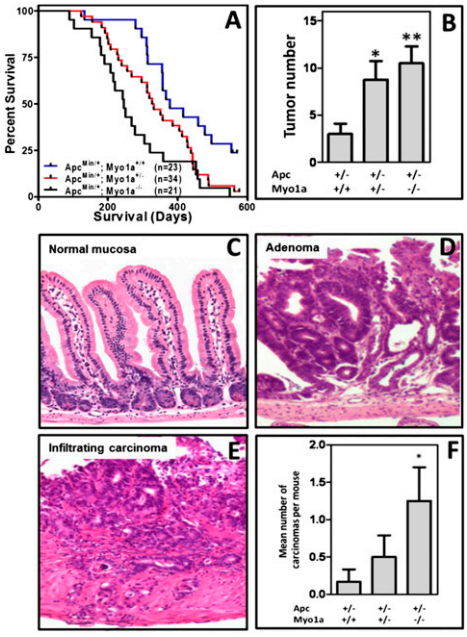

Fig. 3. Role of Myo1a in intestinal tumorigenesis using a murine KO model. The inactivation of one or two copies of *Myo1a* in mice bearing heterozygous mutations of the tumor suppressor gene *Apc* resulted in significantly reduced animal lifespan (*A*). The *P* values of the logrank tests for the comparison of the survival of $Myo1a^{+/-}$ and $Myo1a^{-/-}$ relative to $Myo1a^{+/+}$ animals were $P = 0.022$ and $P = 0.0003$, respectively. (*B*) The number of tumors observed in histological sections of the full small intestine of 30-wk-old $Apc^{Min/+}$;$Myo1a^{-/-}$ ($n = 15$; *t* test, $^{**}P = 0.004$) and $Apc^{Min/+}$;$Myo1a^{+/-}$ ($n = 7$; *t* test, $^{*}P = 0.05$) animals was significantly higher than in the $Apc^{Min/+}$;$Myo1a^{+/+}$ control mice ($n = 11$). Mean ± SD is shown. Examples of the normal small intestine as well as intestinal adenomas and adenocarcinomas are shown in *C*, *D*, and *E*, respectively. Original magnification was 200×. (*F*) The average number of infiltrating adenocarcinomas in 30-wk-old $Apc^{Min/+}$;$Myo1a^{-/-}$ mice was significantly higher than in $Apc^{Min/+}$;$Myo1a^{+/+}$ animals (mean ± SD; Student's *t* test; $^{*}P = 0.05$).

Discussion

Structural proteins of the brush border of the intestinal epithelium have been shown to be lost or reduced during tumor progression (18–20), and this is generally believed to be the result of the loss of differentiation/polarization accompanying this process. However, we show here that the loss of MYO1A drives the tumorigenic process in intestinal tumors. We found frame-shift *MYO1A* mutations in one-third of MSI colorectal tumors and the A8→A7 mutation frequently observed disrupts membrane targeting of MYO1A and interferes with polarization/differentiation of colon cancer cells. Although the promoter region of *MYO1A* does not contain a dense CpG island, methylation of promoter regions that are not within CpG islands has been shown to be important for the regulation of the transcriptional activity (25, 26). We therefore investigated the contribution of CpG methylation to *MYO1A* silencing in colorectal cancer tumor cells and found evidence of *MYO1A* promoter hypermethylation in a significant proportion of colorectal cancer cell lines and primary tumors tested. Moreover, there was an inverse correlation between MYO1A expression and promoter methylation, and treatment with a DNA methyltransferase inhibitor or genetic inactivation of DNA methyltransferase activity led to reduced levels of methylation in the *MYO1A* promoter and increased MYO1A expression in colon cancer cell lines that showed promoter methylation, indicating that promoter hypermethylation is an alternative mechanism of gene silencing in both MSS and MSI colorectal tumors. Ectopic expression of the mutant $MYO1A^{A7}$ form in colon cancer cells that express high endogenous levels of wild-type MYO1A (Caco2 and LS174T cells) leads to a loss of polarization/differentiation, suggesting a dominant-negative effect, probably through the sequestration of additional proteins necessary for the function of the wild-type MYO1A. In good agreement, overexpression of the mutant MYO1A and knockdown of the wild-type endogenous MYO1A phenocopy each other in vitro. However, the lower levels of expression observed in MSI tumors with $MYO1A^{A7}$ mutations suggest that the relevance of the dominant-negative activity of the mutant protein may be limited in primary colorectal tumors.

MYO1A Is Important for STK11/LKB1-Mediated Polarization/Differentiation of Colon Cancer Cells. STK11/LKB1 has been shown to be a key regulator of cell polarity in organisms ranging from yeast to humans. The role of STK11/LKB1 in maintaining the polarity of the intestinal epithelium is highlighted by the fact that germ-line

CELL BIOLOGY

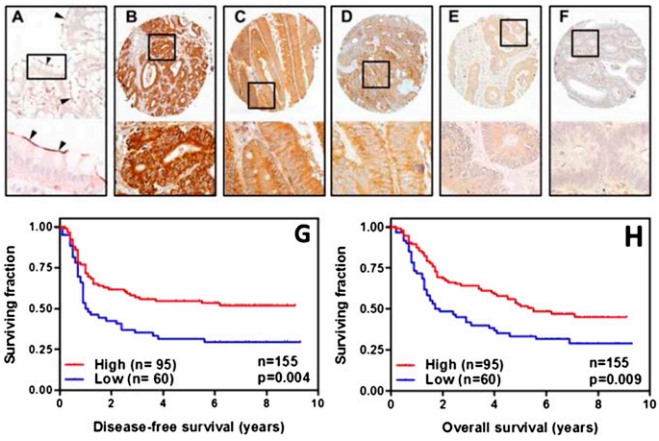

Fig. 4. MYO1A and prognosis of colorectal cancer patients. (*A*) MYO1A immunostaining showed the expected accumulation in the apical brush border of the normal human colonic mucosa (arrowhead). Colorectal human tumors showed variable staining intensity, ranging from levels similar to normal epithelial cells to undetectable levels (*B–F*). (*Lower*) Higher magnification of the indicated regions. Magnification for the upper and lower panels was 200× and 600×, respectively. Kaplan-Meier plots show that patients with low tumor MYO1A levels have shorter disease-free (*G*) (log-rank test, $P = 0.004$) and overall (*H*) (logrank test $P = 0.009$) survival than patients with high tumor MYO1A levels.

mutations of this kinase in humans result in the presence of intestinal hamartomatous polyps and colorectal cancer predisposition (7–9). Although STK11/LKB1 has important functions as a regulator of multiple biological processes and signaling pathways, such as energy metabolism and Wnt or TGF-β signaling, *STK11/LKB1* mutations that do not disrupt its kinase activity but affect its capacity to induce polarization of intestinal epithelial cells are sufficient to cause tumor initiation/progression (10), indicating that the role of STK11/LKB1 in cell polarity is important for intestinal tumor suppression. Here, we demonstrate that MYO1A is important for the STK11/LKB1-dependent polarization/differentiation program of colon cancer cells. Ectopic expression of the mutant MYO1A^{A7} or shRNA-mediated knockdown in LS174T colon cancer cells significantly interferes with their capacity to polarize following STK11/LKB1 activation. Moreover, transfection of MYO1A tail^{A7} into Caco2 cells also interferes with the differentiation program of these cells when grown in confluence, which has also been shown to be STK11/LKB1-dependent (5). Unlike most tumor-suppressor genes that were initially identified as the underlying genetic cause of hereditary cancer predisposition and then found to be frequently mutated in sporadic cancer cases, STK11/LKB1 mutations are rare in sporadic colorectal tumors and epigenetic inactivation is not frequently observed (11–13). Therefore, genetic/epigenetic inactivation of *MYO1A* and other genes downstream of STK11/LKB1 may account for the limited number of STK11/LKB1 mutations observed in sporadic colorectal tumors.

Strict regulation of protein trafficking and vesicle targeting are required for apical-basal polarization of epithelial cells (1, 27). Because Myosin I members have been shown to be important for the targeted delivery of proteins in polarized cells (22, 28, 29), the loss of MYO1A may directly interfere with the subcellular localization of key mediators of cell polarization. Although the detailed molecular mechanisms underlying the role of MYO1A in polarization downstream of STK11/LKB1 remain to be fully elucidated, STK11/LKB1 has been shown to activate AMP-activated protein kinase, which in turn phosphorylates myosin regulatory light chain 2 (MYL12B/MRLC2) (30). MRLC2 phosphorylation seems to be necessary and sufficient for polarization of colon cancer cells (30). Although this myosin light chain has not been reported to directly regulate Myosin Ia, both MRLC2 (30) and MYO1A colocalize with the brush border actin cytoskeleton, providing a possible mechanistic link between MYO1A and polarization of intestinal epithelial cells. Alternatively, the loss of MYO1A-dependent localization of calmodulin to the brush border membrane (24) may affect the phosphorylation state of MRLC2 through aberrant regulation of myosin light-chain kinase.

Loss of MYO1A Is Important for Intestinal Tumorigenesis. Although the molecular mechanisms of the epithelial-to-mesenchymal transition associated with increased metastatic potential of advanced tumors are well characterized, the importance of the loss of polarity/differentiation in tumor cells before the acquisition of metastatic potential is not well understood. Studies in *Drosophila* have convincingly demonstrated that inactivation of genes involved in epithelial cell polarity is important for tumor progression beyond the hyperproliferative stage (1, 3, 4, 31). However, examples of the role of polarity genes in early tumorigenesis of higher vertebrates are scarce. Mice lacking the Lethal giant larvae 1 (*Lgl1*) gene show loss of neural progenitor cell polarity and severe brain dysplasia (32). Furthermore, reduced expression of the key polarity regulators Lgl, Dlg, and Scrib is associated with tumor progression in humans (33–35).

The loss of Myo1a leads to important defects in the differentiation of normal intestinal epithelial cells. As reported previously, in the normal intestine, the loss of Myo1a in the KO mouse causes defects in enterocyte apical membrane tethering, loss of intramicrovillar calmodulin, and the resultant secondary effects of impaired Ca^{2+} homeostasis, mis-targeting of sucrase-isomaltase, destabilization of lipid rafts, and loss of intermicrovillar MYO6 and MYO1E (24). As discussed above, in intestinal tumor cells, the loss of MYO1A interferes with their ability to polarize and differentiate in response to either cell-cell contact or STK11/LKB1 activation. Moreover, in the mouse models used, *Myo1a* inactivation appears to participate in the adenoma-to-carcinoma transition and this is illustrated by a significantly higher incidence of locally invasive carcinomas in the intestine of *Myo1a* KO mice compared with *Myo1a* wild-type mice following tumor initiation by *Apc* mutations. However, the inactivation of *Myo1a* in *Apc*$^{Min/+}$ mice did not lead to a metastatic phenotype. In human tumors, the loss of MYO1A seems to contribute to the acquisition of local invasive capacity. This finding is consistent with the observation that mutation frequency significantly increases as tumors progress from a benign adenoma to a locally invasive carcinoma (Dukes B) (*SI Appendix*, Fig. S1*D*). However, no further increase in mutation frequency was observed in late-stage tumors that have metastasized to either regional lymph nodes (Dukes C) or distant organs (Dukes D) compared with locally invasive tumors (Dukes B). Moreover, we found no differences in the levels of MYO1A protein expression in Dukes C primary tumors and matched lymph node metastases, further indicating that the loss of MYO1A does not significantly contribute to tumor metastasis.

MYO1A Is an Independent Marker of Prognosis for Colorectal Cancer Patients. The prognosis of colorectal cancer patients is largely determined by tumor staging based on the degree of penetration of the tumor through the intestinal wall and the presence of metastasis in regional lymph nodes or distant organs. However, patients diagnosed with histopathologically indistinguishable tumors of the same stage can widely vary in their survival, highlighting the need for additional markers allowing stratification of patients with different prognosis. Here we show that the tumor levels of MYO1A in patients diagnosed with Dukes C colorectal cancer were significantly associated with patient survival. The disease-free survival of patients that retained high tumor levels of MYO1A was >ninefold longer than patients with low MYO1A tumor levels (>9.1 vs. 1.0 y respectively), indicating that MYO1A levels can be used to predict the probability of patient survival.

In conclusion, these results demonstrate that structural proteins of the intestinal brush border, previously believed to be passive differentiation markers in colorectal tumors, can actively

contribute to tumor progression. Therefore, our results indicate that further investigation of the oncogenic effects of the loss of additional putative differentiation markers is warranted in colorectal tumors and possibly other tumor types. The results of the mouse KO models and the genetic data from human colorectal tumors significantly contribute to elucidate the emerging role of genes involved in epithelial cell polarity/differentiation on epithelial tumorigenesis.

Materials and Methods

Cell lines and clinical samples: All cell lines were maintained in DMEM medium supplemented with 10% FBS and 1× antibiotic antimycotic (Invitrogen). The clinicopathological data of the 134 MSI patients used for the *MYO1A* mutation screening and the 155 patients in the tissue microarray used for MYO1A immunostaining are summarized in Tables S1 and S3, respectively. Sequencing: *MYO1A* mutations were assessed by direct sequencing of *MYO1A* exon 28. Fluorescence microscopy: Caco2 and LS174T-W4 cells were grown on gelatinized coverslips and transfected (Lipofectamine 2000) with the indicated vectors. Images were captured with a confocal microscope (Olympus FV1000). Enzymatic activity assays: The activity of alkaline phosphatase (AP), sucrase isomaltase (SI), and dipeptidyl peptidase-4 (DPP4) in Caco-2 cells that were confluent for 0, 2, 5, 7, 14, or 21 days was assessed as previously described. Xenograft model: Caco2 and SW403 cells transduced with shMYO1A and control nontarget shRNA (shNT) were s.c. injected in athymic nude mice. Tumor growth was monitored for 7 wk. Mouse knockout strains: *Myo1a* KO mice were used to investigate the role of Myo1a in tumor progression initiated by Apc mutations ($Apc^{min/+\ model}$) or azoxymethane treatment (nine weekly i.p. injections of 10 mg/kg). Immunohistochemistry and Western blotting: Immunohistochemical staining of formalin-fixed, paraffin embedded samples following antigen retrieval with 10 mM citrate buffer pH 6.0 [anti-BrdU, Developmental Studies Hybridoma Bank; anti-MYO1A (24)] or 1 mM EDTA (lysozyme, Dako). Anti-GAPDH (1:1000; clone 6C5; Santa Cruz) was used as a loading control in Western blot analysis. CpG methylation assays and Real-Time RT-PCR: The Infinium quantitative methylation assay (Illumina) was used following manufacturer's instructions. For bisulfite sequencing, DNA was treated with bisulfite and sequenced. MYO1A promoter methylation and expression levels of primary colorectal tumors were obtained from The Cancer Genome Atlas (http://cancergenome.nih.gov/). For qPCR, total RNA was extracted and reverse transcribed, and relative MYO1A mRNA levels assessed by real-time PCR using SYBR Green Master Mix (Applied Biosystems). 18S rRNA was used as a standardization control for the 2-ΔΔCt method. Primer sequence and PCR conditions can be found in Table S5. Additional materials and methods are described in *SI Materials and Methods*.

ACKNOWLEDGMENTS. LS174T-W4 cells were a kind gift of Dr. Hans Clevers (Hubrecht Laboratory and Centre for Biomedical Genetics, Utrecht, The Netherlands). The BrdU hybridoma developed by Dr. Stephen J. Kaufman was obtained from the Developmental Studies Hybridoma Bank developed under the auspices of the National Institute of Child Health and Human Development and maintained by The University of Iowa, Department of Biology. This study was partially funded by Grants CP05/00256, TRA2009-0093, and SAF2008-00789 of the Spanish Ministry of Science and Innovation, and Fundación Mutua Madrileña and Agència de Gestió d'Ajuts Universitaris i de Recerca SGR 157 (to D.A.), and by National Institutes of Health Grant DK 25387 (to M.S.M.).

1. Wodarz A, Näthke I (2007) Cell polarity in development and cancer. *Nat Cell Biol* 9: 1016–1024.
2. Thiery JP (2002) Epithelial-mesenchymal transitions in tumour progression. *Nat Rev Cancer* 2:442–454.
3. Wodarz A (2000) Tumor suppressors: Linking cell polarity and growth control. *Curr Biol* 10:R624–R626.
4. Partanen JI, Nieminen AI, Klefstrom J (2009) 3D view to tumor suppression: Lkb1, polarity and the arrest of oncogenic c-Myc. *Cell Cycle* 8:716–724.
5. Baas AF, et al. (2004) Complete polarization of single intestinal epithelial cells upon activation of LKB1 by STRAD. *Cell* 116:457–466.
6. Baas AF, Smit L, Clevers H (2004) LKB1 tumor suppressor protein: PARtaker in cell polarity. *Trends Cell Biol* 14:312–319.
7. Hemminki A, et al. (1998) A serine/threonine kinase gene defective in Peutz-Jeghers syndrome. *Nature* 391:184–187.
8. Jeghers H, Mckusick VA, Karz KH (1949) Generalised intestinal polyposis and melanin spots of oral mucosa, lips and digits: A syndrome of diagnostic significance. *N Engl J Med* 241:992–1005.
9. Peutz JL (1921) On a very remarkable case of familial polyposis of the mucuous membrane of the intestinal tract and nasopharynx accompanied by peculiar pigmentation of the skin and mucuous membranes. *Ned Tijdschr Geneeskd* 10:134–146.
10. Forcet C, et al. (2005) Functional analysis of Peutz-Jeghers mutations reveals that the LKB1 C-terminal region exerts a crucial role in regulating both the AMPK pathway and the cell polarity. *Hum Mol Genet* 14:1283–1292.
11. Esteller M, et al. (2000) Epigenetic inactivation of LKB1 in primary tumors associated with the Peutz-Jeghers syndrome. *Oncogene* 19:164–168.
12. Trojan J, Brieger A, Raedle J, Esteller M, Zeuzem S (2000) 5′-CpG island methylation of the LKB1/STK11 promoter and allelic loss at chromosome 19p13.3 in sporadic colorectal cancer. *Gut* 47:272–276.
13. Wang ZJ, Taylor F, Churchman M, Norbury G, Tomlinson I (1998) Genetic pathways of colorectal carcinogenesis rarely involve the PTEN and LKB1 genes outside the inherited hamartoma syndromes. *Am J Pathol* 153:363–366.
14. Cheng H, Leblond CP (1974) Origin, differentiation and renewal of the four main epithelial cell types in the mouse small intestine. V. Unitarian Theory of the origin of the four epithelial cell types. *Am J Anat* 141:537–561.
15. Barker N, et al. (2007) Identification of stem cells in small intestine and colon by marker gene Lgr5. *Nature* 449:1003–1007.
16. Sangiorgi E, Capecchi MR (2008) Bmi1 is expressed in vivo in intestinal stem cells. *Nat Genet* 40:915–920.
17. Bement WM, Mooseker MS (1996) The cytoskeleton of the intestinal epithelium: Components, assembly, and dynamic rearrangements. *The Cytoskeleton of Spacialized Tissues and Pathological States*, eds Hesketh J, Pryme I (IJAI Press, Greenwich, CT), Vol 3, pp 689–404.
18. Chantret I, Barbat A, Dussaulx E, Brattain MG, Zweibaum A (1988) Epithelial polarity, villin expression, and enterocytic differentiation of cultured human colon carcinoma cells: A survey of twenty cell lines. *Cancer Res* 48:1936–1942.
19. Beaulieu JF, Weiser MM, Herrera L, Quaroni A (1990) Detection and characterization of sucrase-isomaltase in adult human colon and in colonic polyps. *Gastroenterology* 98:1467–1477.
20. West AB, et al. (1988) Localization of villin, a cytoskeletal protein specific to microvilli, in human ileum and colon and in colonic neoplasms. *Gastroenterology* 94:343–352.
21. Colluccio LM (2008) MYOSIN I. *Myosins: A Superfamily of Molecular Motors*, ed Colluccio LM (Springer, Dordrecht, The Netherlands), pp 95–124.
22. Tyska MJ, Mooseker MS (2004) A role for myosin-1A in the localization of a brush border disaccharidase. *J Cell Biol* 165:395–405.
23. Ramond MJ, Martinot-Peignoux M, Erlinger S (1985) Dome formation in the human colon carcinoma cell line Caco-2 in culture. Influence of ouabain and permeable supports. *Biol Cell* 54:89–92.
24. Tyska MJ, et al. (2005) Myosin-1a is critical for normal brush border structure and composition. *Mol Biol Cell* 16:2443–2457.
25. Irizarry RA, et al. (2009) The human colon cancer methylome shows similar hypo- and hypermethylation at conserved tissue-specific CpG island shores. *Nat Genet* 41: 178–186.
26. Han H, et al. (2011) DNA methylation directly silences genes with non-CpG island promoters and establishes a nucleosome occupied promoter. *Hum Mol Genet* 20: 4299–4310.
27. Nelson WJ, Yeaman C (2001) Protein trafficking in the exocytic pathway of polarized epithelial cells. *Trends Cell Biol* 11:483–486.
28. Krendel M, Mooseker MS (2005) Myosins: Tails (and heads) of functional diversity. *Physiology (Bethesda)* 20:239–251.
29. Nambiar R, McConnell RE, Tyska MJ (2009) Control of cell membrane tension by myosin-I. *Proc Natl Acad Sci USA* 106:11972–11977.
30. Lee JH, et al. (2007) Energy-dependent regulation of cell structure by AMP-activated protein kinase. *Nature* 447:1017–1020.
31. Bilder D, Li M, Perrimon N (2000) Cooperative regulation of cell polarity and growth by *Drosophila* tumor suppressors. *Science* 289:113–116.
32. Klezovitch O, Fernandez TE, Tapscott SJ, Vasioukhin V (2004) Loss of cell polarity causes severe brain dysplasia in Lgl1 knockout mice. *Genes Dev* 18:559–571.
33. Kuphal S, et al. (2006) Expression of Hugl-1 is strongly reduced in malignant melanoma. *Oncogene* 25:103–110.
34. Nakagawa S, et al. (2004) Analysis of the expression and localisation of a LAP protein, human scribble, in the normal and neoplastic epithelium of uterine cervix. *Br J Cancer* 90:194–199.
35. Schimanski CC, et al. (2005) Reduced expression of Hugl-1, the human homologue of *Drosophila* tumour suppressor gene lgl, contributes to progression of colorectal cancer. *Oncogene* 24:3100–3109.

SUPPORTING INFORMATION

Brush Border Myosin Ia Has Tumor Suppressor Activity in the Intestine

Rocco Mazzolini[1,2], Higinio Dopeso[1,2]*, Silvia Mateo-Lozano[1,2]*, Wakam Chang[3], Paulo Rodrigues[1,2], Sarah Bazzocco[1], Hafid Alazzouzi[1], Stefania Landolfi[4], Javier Hernandez-Losa[4], Elena Andretta[1,2], Pia Alhopuro[5], Eloy Espín[6], Manel Armengol[6], Josep Tabernero[7], Santiago Ramón y Cajal[4], Matthias Kloor[8], Johannes Gebert[8], John M. Mariadason[9], Simo Schwartz Jr[2,10], Lauri A. Aaltonen[5], Mark S. Mooseker[3], Diego Arango[1,2].

SUPPORTING MATERIALS AND METHODS

Cell lines and clinical samples. All the colorectal cancer cell lines used in this study (see **Table S2**) were maintained on Dulbecco's modified Eagle's medium (DMEM; PAA Laboratories) containing 10% fetal bovine serum (PAA Laboratories) and 1x antibiotic-antimycotic (Invitrogen; 10,000 U penicillin, 10,000 µg of streptomycin, and 25 µg/ml of amphotericin B) at 37^0C/5% CO_2. LS174T-W4 cells were a kind gift of Dr. Hans Clevers (Hubrecht Laboratory and Centre for Biomedical Genetics, Utrecht, the Netherlands). SW403 and Caco2 cells were stably transduced with short-hairpin RNAs by lentiviral infection (MISSION shRNA Vectors TRCN0000083865 and TRCN0000083866; Sigma) and subsequently selected with puromycin (Invitrogen; 4µg/ml and 20µg/ml respectively). RKO cells were stably transduced with pRECEIVER-Lv19-EGFP-MYO1A or the corresponding empty vector control pRECEIVER-Lv19 by lentiviral infection (Genecopoeia) and selected with G418 (500µg/µl; Invitrogen).

Primary colorectal tumor samples were collected at collaborating medical institutions in Spain and Finland. Informed consent for genetic analysis of the tumor sample was obtained from each patient, according to protocols approved by the Human Investigations and Ethical Committee in the appropriate Institution. For *MYO1A* mutation screening, DNA was extracted from 36 MSI colorectal cancer cell lines as well as fresh frozen tumor and matched normal mucosa samples from 134 MSI colorectal cancer cases. The clinicopathological features of these patients are shown in **Table S1**. A tissue microarray containing triplicate samples from 155 colorectal cancer tumors (4) was used for immunohistochemical assessment of MYO1A levels (mean follow up of 8.7 years; range from 6.8 to 11.2 years). The clinicopathological features of these patients are shown in **Table S3**.

Sequencing. *MYO1A* mutations were screened by direct sequencing of PCR amplified genomic DNA (ABI Prism 3100 sequencer; Applied Biosystem). PCR primers and conditions are detailed in **Table S5**.

Fluorescence microscopy. Cells were grown on gelatine-coated glass coverslips. Caco2 cells were transfected (Lipofectamine 2000; Invitrogen) with the vectors MYO1A EGFP-tail^{wt} or MYO1A EGFP-tail^{A7MUT} containing the tail-domain of MYO1A (amino acids 772 to 1043). Cells were non-confluent or maintained 3 weeks in confluence to induce full differentiation, fixed in 4% paraformaldehyde, permeabilized with 0.1% Triton X-100 and stained with rhodamine-phalloidin (0.1uM; Cytoskeleton). Orthogonal sections were obtained with a confocal microscope (FV1000 Olympus).

LS174T-W4 cells were transfected with EGFP-MYO1A^{A7MUT}, EGFP-MYO1A^{wt}, shMYO1A/pEGFP-C2 plasmids in parallel with the pEGFP-C2 (Clontech) or non-target shRNA (Mission, Sigma) respective control vectors. LKB1/STK11 expression leading to a polarized phenotype(5) was induced by doxycyclin treatment (5µg/ml). Cells were fixed with 4% paraformaldehyde 24h after doxycyclin treatment and stained with rhodamine-phalloidin (0.1uM; Cytoskeleton). The number of polarized EGFP-positive cells was scored using a fluorescent microscope (Olympus

BX61 equipped with a camera DP70). Polarized cells were defined by the characteristic accumulation of actin in one pole of the cell as previously described and shown to be associated with brush border formation and sorting of apical and basolateral markers(5). Over 450 EGFP-positive cells were scored blinded from the sample ID in three independent experiments.

Enzymatic activity assays. Caco2 cells were grown for 0, 2, 5, 7, 14 and 21 days post-confluence, and total cellular lysates extracted with mannitol buffer (50mM D-mannitol, 2mM Tris and 0.1% Triton X-100) containing protease inhibitors (0.3mM phenylmethylsulfonyl fluoride, 1ug/ml aprotinin, 100uM sodium ortovanadate, 5ug/ml pepstatin). SW403 cells were exposed to 5mM Sodium Butyrate for 72h. Alkaline phosphatase (AP), sucrase isomaltase (SI) and dipeptidyl peptidase-4 (DPP4) activity were determined. Briefly, for AP activity assay 50µg of protein (in a volume of 50µl of mannitol buffer) were mixed with 200µl of p-Nitrophenyl Phosphate Liquid Substrate System (Sigma N7653), incubated at 37^0C for 15 min and the absorbance was measured at 405nm. For SI activity, 25ug of protein in 12.5µl of mannitol buffer were incubated with an equal volume of substrate (maltose 0.056M in mannitol buffer, pH 6.0) at 37^0C for 60 min. The reaction was stopped by heating at 100^0C for 2 min and the precipitate was resuspended on 250µl of TGO buffer (horseradish peroxidase 5mg, glucose oxidase 4mg, o-dianisidine 10mg and 0.2 % Triton X-100 in a final volume of 100ml of Tris 0.5M, pH 7.0) and the absorbance measured at 450nm. For DPP4 activity assay, 50µg of protein in 90µl of mannitol buffer were added to 10µl of 1.4M glycine-NaOH pH 8.7 and incubated in the presence of 100µl of substrate (glycyl-L-proline-p-nitroanilide, final 1.5mM) at 37^0C for 30min. The reaction was stopped with 800µl of 32% trichloroacetic acid and samples were centrifuged at 1700rcf for 10min. Then, 50µl of supernantant were added to 50µl of cold 0.2% sodium nitrite and incubated at 4^0C for 10min. Next, 50µl of 0.5% ammonium sulfamate were added and after 2min of incubation, 100µl of 0.05% n-(1-naphthyl)-ethanediamine were added and incubated at 37^0C for 30min in the dark. The absorbance was read at 548nm. All these experiments were carried out at least three independent times in triplicate.

Dome formation in Caco2 cells. Caco2 cells were grown for 21 days in confluence in a 6-well plate. The number of domes was directly counted blinded from the sample ID using an inverted microscope in three independent experiments in triplicate.

Western blot. Total cellular lysates (RIPA buffer) were subjected to SDS–PAGE on a 10% gel and transferred to PVDF membranes as described before(6) and hybridized using antibodies against human MYO1A (1:1000; see reference(7)) and GAPDH (1:1000; clone 6C5; Santa Cruz).

Soft agar colony formation assay. Cells (1×10^5) were resuspended in complete DMEM medium containing 0.3% agar and then plated onto six-well plates on top of 0.6% agar in DMEM medium. Cultures were maintained at 37°C in a 5% CO_2 incubator for 21 days. The colonies were stained with nitrotetrazolium blue chloride (1mg/ml; Sigma) and the number of macroscopically visible colonies was scored. Three independent experiments in triplicate were carried out.

Xenograft model. All animal experiments were carried out under protocols approved by the Institutional Ethical Committee and the corresponding governmental agency. Six athymic nude-*Foxn1*^{nu} mice (Harlan Laboratories) were injected s.c. with $3x10^6$ SW403-shNT (left flank) and SW403-shMYO1A (right flank) cells resuspended in 100µl of PBS. The same experimental setup was used for the Caco2-shMYO1A derivative line and the corresponding non-target shRNA control (shRNA vectors from Mission, Sigma). Tumor size was measured using a caliper three times per week for a total of 7 weeks. Tumor volume was calculated with the formula: $V = (LxW^2)x0.5$, where L is the length and W is the width of a xenograft.

Mouse knockout strains. The C57BL/6J-Apc^{min}/J strain was obtained from The Jackson Laboratory. These mice carry a heterozygous mutation in *Apc*. 129X1/SvJ-Myo1a mice carry *Myo1a* alleles in

which a neo/URA3 cassette replaced the first three *Myo1a* exons. Male $Apc^{min/+;}Myo1a^{+/+}$ mice were crossed with female $Apc^{+/+;}Myo1a^{-/-}$ mice to obtain $Apc^{min/+;}Myo1a^{+/-}$ males and $Apc^{+/+;}Myo1a^{+/-}$ females that were subsequently crossed to obtain the $Apc^{min/+};Myo1a^{+/+}$, $Apc^{min/+};Myo1a^{+/-}$ and $Apc^{min/+};Myo1a^{-/-}$ offspring with an equal contribution of the 129Sv and C57BL/6 genetic background that were used in the experiments described. Nine-week old $Myo1a^{+/+}$ and $Myo1a^{-/-}$ (both $Apc^{+/+}$ on a pure 129X1/SvJ background) mice were i.p. injected with the intestine-specific carcinogen azoxymethane (AOM; 10mg/kg) weekly for 9 weeks and sacrificed 10 weeks after the last AOM injection.

Histology and immunohistochemistry. Thirty-week-old mice were sacrificed, the small and large intestine were dissected, opened longitudinally, and the number and size of macroscopically visible tumors scored under the dissecting microscope. The tissue was then fixed overnight with 10% formalin, transferred to a tissue cassette and dehydrated by serial immersion in 50%, 70%, 96% and 100% ethanol. Excess ethanol was removed by incubation in xylene three times for 1h at room temperature and the cassettes then immersed in 65^0C paraffin overnight. Paraffin blocks of the whole small or large intestine were prepared using the 'Swiss Roll' approach as previously described (8) and tumor multiplicity was also determined on Hematoxylin and Eosin stained tissue sections.

For immunohistochemistry (IHC), tissue sections (4µm) were cut and placed on poly-L-Lysine coated microscope slides, incubated at 54^0C for 1h and de-waxed by immersion in xylene (2x5 min) and hydrated by serial immersion in 100% EtOH (2x5 min), 96% EtOH (5 min), 70% EtOH (5 min), 50% EtOH (5 min) and distilled water. The NovoLink polymer detection system (Novocastra Laboratories) was used according to manufacturer's instructions. For BrdU staining, 10mM citrate buffer pH 6.0 for 20 min at 120^0C in autoclave was used for sample antigen retrieval and then incubated with mouse monoclonal anti-BrdU primary antibody (1/16 hybridoma supernatant; Developmental Studies Hybridoma Bank). The position of BrdU-positive cells 24h post-administration was scored (position 0 being at the bottom of the crypt). Antigen retrieval for lysozyme IHC (N1515; Dako; ready to use) was done in 100^0C 1mM EDTA (10 min). For MYO1A staining, antigen retrieval was done in 10mM citrate buffer (pH 6.0) in a microwave oven (5min at 800 watt and 10 minutes at 400 watt). Sections were incubated with rabbit polyclonal anti-MYO1A(7) (1.5µg/ml) at 4^0C overnight. Slides were counterstained with Mayer's haematoxylin dehydrated and mounted with in DPX mounting medium (Panreac Química). MYO1A immunostaining intensity was assessed in triplicate tumor samples from the 155 patients with locally advanced colorectal cancer (Dukes C) in the tissue microarray. A semi-quantitative scale from 0 to 4 was used to assess staining intensity blinded from the clinicopathological data. Absence of MYO1A immunostaining was scored as 0 and increasing MYO1A levels were scored as 1, 2, 3 or 4 (see **Figure 4B-F**). The average score of triplicate samples was used in subsequent analyses. In some analyses, MYO1A levels were dichotomized as low if average immunostaining score was <2.3 and high if it was ≥2.3. To select this cutoff value we systematically assessed the survival difference in the high and low MYO1A groups for every possible cutoff value observed in this series, and selected the value that maximized the survival differences (see **Table S4**). Although the p value (Logrank test) varied depending on the cutoff selected, the group of patients with high MYO1A tumor levels always showed longer disease-free and overall survival than patients in the low MYO1A group, indicating that the survival differences are independent of the immunostaining cutoff selected (see **Table S4**). In other analyses, the level of MYO1A was considered as a continuous variable and Cox multivariate regression analysis was used to confirm independent prognostic factors for these patients (covariates: MYO1A tumor levels, patient age, sex, adjuvant treatment, tumor location and grade). This further demonstrates that the survival differences between the high and low MYO1A groups of the earlier analyses are not

dependent on the immunostaining cutoff selected.

Goblet cell staining was done with 1% alcian blue (Sigma) in 3% acetic acid for 30min and counterstained with hematoxylin. Enteroendocrine cells were stained using Grimelius silver staining. Briefly, sections were dewaxed, rehydrated, post-fixed with Bouin's solution (Sigma) for 1h at 37^0C, rinsed once in 70% EtOH, twice in distilled water and immersed in silver solution (0.5% silver nitrate in 0.1M acetate buffer pH 5.8) for 3-4 h at 60^0C. Then sections were immersed in Bodian solution (5% anhydrous sodium sulfate and 1% hydroquinone in water) for 5 minutes at 60^0C, fixed in 2% sodium thiosulphate, washed in PBS, dehydrated and mounted.

CpG methylation assays. The Infinium quantitative methylation assay (Illumina) was used following manufacturer's instructions. Briefly, after bisulfite treatment the genomic DNA is subjected to whole genome amplification and allele specific oligonucleotides detect the methylated and unmethylated cytosine in two CG dinucleotides located -154bp and +271bp relative to the transcription start site. DNA methylation in the CpG dinucleotide located in position -154bp was independently confirmed in 10 colorectal cancer cell lines using bisulfite sequencing. DNA was isolated from each line using DNAzol (Molecular Research Center) according to the manufacturer's recommendations. For bisulfite sequencing, DNA (1µg in 50µl water) was denaturated by alkaline treatment (by adding 7µl of NaOH 3M for 15min at 37ºC) and deaminated (by adding 33µl hydroquinone 20mM and 530µl of sodium bisulfite 3M pH5, for 16h at 50^0C). Then DNA was purified (DNA Wizard kit, Promega), incubated with 5.7µl of NaOH 3M for 10min at RT, neutralized with 17µl of 10M ammonium acetate and ethanol precipitated. DNA was then PCR-amplified and the 174bp fragment was sequenced using BigDye Terminator 1.1 and an ABI PRISM 3100 sequencer (Applied Biosystems, Foster City, CA). Primers for DNA amplification and sequencing were designed using MethPrimer 1.1 software (see **Table S5** for primers sequence). Methylated cytosine residues are protected from bisulfite treatment and were observed as cytosine after sequencing, whereas unmethylated cytosines were detected as thymidine residues. For the effects of DNA methyltransferase inhibition either genetically or pharmacologically on *MYO1A* promoter methylation in HCT116 cells we used data publicly available (ArrayExpress E-MTAB-210 (3) and Gene Expression Omnibus GSE26990 (2)). MYO1A promoter methylation and expression levels of primary colorectal tumors were obtained from The Cancer Genome Atlas (http://cancergenome.nih.gov/).

5-aza-2'-deoxycytidine treatment and Real-Time RT-PCR. Cells were grown in complete DMEM medium as described above containing 5-aza-2'-deoxycytidine (0, 2.5 or 10µM; Sigma) for 72 hours. Medium was replaced every 24 hours. Total RNA was extracted from control and 5-aza-2'-deoxycytidine treated cells, using the TRI Reagent (Molecular Research Center) according to the manufacturer's instruction. Total RNA (500ng) was reverse transcribed using the High Capacity cDNA Reverse Transcription kit (Applied Biosystems), and relative MYO1A mRNA levels were assessed by Real-Time PCR using SYBR Green Master Mix (Applied Biosystems, Branchburg, NJ). 18S rRNA was used as a standardization control for the $2^{-\Delta\Delta Ct}$ method as described before(4). Primer sequence and PCR conditions can be found in **Table S5.** For 5-Aza-2'-deoxycytidine treated Co115 cells the product of the PCR amplification of bisulfite-converted *MYO1A* promoter regions was cloned suing the CloneJET PCR Cloning Kit (Thermo Scientific) according to manufacturer's instructions and sequenced as described above.

Statistical Methods. Data are presented as mean ± standard error (SE) or standard deviation (SD), as indicated. For the survival analysis, Kaplan-Meier curves were analyzed using the logrank test (GraphPad Prism 5.0). To assess the significance of the mutation frequency of *MYO1A* in MSI tumors, a logistic regression model was used with 62 control intronic repeats as described (1). For comparison of the clinicopathological data the Fisher's exact test, Mann Whitney test, Chi2 test

or Cox multivariate regression analysis was used, as indicated (SSPS Statistics 17.0, IBM). $p < 0.05$ was considered significant.

1. Alhopuro P*, et al.* (2010) Mutations in the Circadian Gene *CLOCK* in Colorectal Cancer. *Mol Cancer Res* 8(7):952-960.
2. Sproul D*, et al.* (2011) Transcriptionally repressed genes become aberrantly methylated and distinguish tumors of different lineages in breast cancer. *Proc Natl Acad Sci U S A* 108(11):4364-4369.
3. Hagemann S, Heil O, Lyko F, & Brueckner B (2011) Azacytidine and decitabine induce gene-specific and non-random DNA demethylation in human cancer cell lines. *PLoS ONE* 6(3):e17388.
4. Arango D*, et al.* (2005) Gene-expression profiling predicts recurrence in Dukes' C colorectal cancer. *Gastroenterology* 129(3):874-884.
5. Baas AF*, et al.* (2004) Complete polarization of single intestinal epithelial cells upon activation of LKB1 by STRAD. *Cell* 116(3):457-466.
6. Dopeso H*, et al.* (2009) The receptor tyrosine kinase EPHB4 has tumor suppressor activities in intestinal tumorigenesis. *Cancer Res* 69(18):7430-7438.
7. Tyska MJ*, et al.* (2005) Myosin-1a is critical for normal brush border structure and composition. *Mol Biol Cell* 16(5):2443-2457.
8. Moolenbeek C & Ruitenberg EJ (1981) The "Swiss roll": a simple technique for histological studies of the rodent intestine. *Lab Anim* 15(1):57-59.

Supporting Table 1: Clinicopathological features of colorectal cancer patients with MSI tumors analyzed for mutations in the A8 track of *MYO1A* exon 28.

	Total	*Mutant MYO1A*	*Wild type MYO1A*	*p value*
MYO1A levels (IHC score), mean±SD	2.7±1.1	2.1±0.9	3.1±0.9	0.03[2]
Sex, n (%)				
Female	73	24 (32.8)	49 (67.2)	0.44[1]
Male	58	15 (25.8)	43 (74.2)	
Age (years), mean±SD	63.4±15.7	62.9±15.3	63.6±16.0	0.75[2]
Degree of diffirentiation, n (%)				
Good	19	8 (42.1)	11 (57.9)	0.14[3]
Moderate	71	26 (36.6)	45 (63.4)	
Poor	39	8 (20.5)	31 (79.5)	
Dukes Stage, n (%)				
Adenomas	17	2 (11.7)	15 (88.3)	0.04[4]
Dukes A	41	9 (21.9)	32 (78.1)	
Dukes B	57	20 (35)	37 (65)	
Dukes C	32	11 (34.3)	21 (65.7)	
Dukes D	3	1 (33.3)	2 (66.7)	
Mean follow up (years), mean±SD	8.4±2.1	9.1±0.9	8.1±2.4	0.42[2]
5-year overall survival, n (%)				
Alive	58	22 (37.9)	36 (62.1)	0.23[1]
Dead	30	7 (23.3)	23 (76.7)	

[1]Fisher's exact test, [2]Mann Whitney test, [3]Chi2 test and [4]Chi2 test comparing adenomas/Dukes A vs. Dukes B-D.

Supporting Table 2: MYO1A mRNA levels, MYO1A[7A] mutations and CpG methylation (beta methylation values). The β-value represents a continuous measurement from 0 (completely unmethylated) to 1 (completely methylated). β-value = (signal intensity of methylation-detection probe)/(signal intensity of methylation-detection probe + signal intensity of non-methylation-detection probe).

Cell line	MSI[1]	CG -154 Infinium[2]	CG+271 Infinium[3]	CG -154 Bisulfite seq[4]	MYO1A mRNA levels[5]	MYO1A Ex28 A8 mutations
RKO	MSI	0.87	0.63	Methylated	0.04	A8/A8
SW48	MSI	0.87	0.84		0.07	A8/A7
SW480	MSS	0.87	0.84	Methylated	0.17	
LIM2405	MSI	0.85	0.48		0.15	A8/A7
HCT15	MSI	0.78	0.66		0.12	A8/A7
HCT116	MSI	0.78	0.81	Methylated	0.08	A8/A8
DLD1	MSI	0.73	0.60	Methylated		A8/A8
HCC2998	MSS	0.71	0.36		2.88	
Vaco5	MSI	0.67	0.78	Methylated		A8/A8
Colo320	MSS	0.65	0.21		0.05	
HCA7	MSI	0.64	0.31			A8/A8
HT29	MSS	0.63	0.18		0.41	
TC71	MSI	0.63	0.77			A8/A7
FET	MSS	0.62	0.35			
Co115	MSI	0.61	0.72	Methylated		A8/A8
SKCO1	MSS	0.59	0.28		0.19	
LIM1215	MSI	0.59	0.17		1.86	A8/A8
IS1	MSS	0.57	0.37			
SW620	MSS	0.57	0.37		0.58	
HDC75	MSS	0.55	0.45			
HDC108	MSI	0.52	0.04			A8/A8
SW837	MSS	0.52	0.11		1.1	
HDC9	MSI	0.50	0.15			A8/A7
GP5D	MSI	0.50	0.65			A8/A7
LOVO	MSI	0.47	0.11		9.22	A8/A8
HDC114	MSS	0.42	0.22			
Ala	MSS	0.41	0.35			
Caco2	MSS	0.40	0.24		1.55	
Colo201	MSS	0.39	0.05		0.08	
Colo205	MSS	0.38	0.04		15.96	
SW948	MSS	0.30	0.03		3.99	
KM12	MSI	0.28	0.64		0.06	A8/A7
V9P	MSS	0.27	0.05			
HDC111	MSS	0.20	0.07			
LS1034	MSS	0.19	0.03			
RW2982	MSS	0.17	0.05		3.36	
T84	MSS	0.17	0.02		1.81	
HDC15	MSS	0.16	0.06			
LS513	MSS	0.15	0.03			
HDC87	MSS	0.13	0.25			
IS2	MSS	0.13	0.03			
SW1116	MSS	0.12	0.03		8.93	
LS174T	MSI	0.09	0.12	Un-methylated	2.33	A8/A8
IS3	MSS	0.09	0.05	Un-methylated		
RW7213	MSS	0.08	0.03	Un-methylated	3.19	
SW403	MSS	0.07	0.03	Un-methylated	14.15	

[1]Microsatellite status: MSS, miscrosatellite stable; MSI, microsatellite instable; [2]Results of quantitative Infinium assay for the CpG dinucleotide located in position -154bp relative to MYO1A transcription start site (TSS); [3]Results of quantitative Infinium assay for CpG dinucleotide located in position +271bp relative to MYO1A TSS; [4]Results of bisulfite sequencing of the region containing the CpG dinucleotide located in position -154bp relative to MYO1A TSS (methylated: unmethylated peak in the chromatograms is <20%; un-methylated: methylated peak in the chromatograms is <20%); [5]relative mRNA levels assessed by quantitative Real-Time RT PCR.

Supporting Table 3: Clinicopathological features of the 155 colorectal cancer patients analyzed for tumor levels of MYO1A protein.

	Total	*High MYO1A*	*Low MYO1A*	*p value*
Sex, n (%)				
Female	76	50 (65.8)	26 (34.2)	0.7[1]
Male	79	45 (57)	34 (43)	
Age (years), mean±SD	64.7±12.9	63.4±12.6	66.7±13.2	0.09[2]
Site, n (%)				
Colon	93	62 (66.7)	31 (33.3)	0.09[1]
Rectum	61	32 (52.5)	29 (47.5)	
Degree of diffirentiation, n (%)				
Good	20	11 (55)	9 (45)	0.13[1]
Moderate	112	66 (59)	46 (41)	
Poor	21	17 (81)	4 (19)	
Mean follow up (years), mean±SD	9.2±1.1	9.2±1.1	9.2±1.1	0.78[2]
Adjuvant treatment, n (%)				
Yes	81	54 (66.7)	27 (33.3)	0.14[1]
No	73	40 (54.8)	33 (45.2)	
5-year overall survival, n (%)				
Alive	70	50 (71.5)	20 (28.5)	0.02[1]
Dead	85	45 (53)	40 (47)	
5-year disease-free survival, n (%)				
Alive	73	52 (71.3)	21 (28.7)	0.013[1]
Dead	80	41 (51.3)	39 (48.7)	

[1]Fisher's exact test; [2]Mann Whitney test.

Supporting Table 4: Mean disease-free and overall survival as a function of the IHC score used as a cutoff to define the high and low MYO1A groups of patients. All possible cutoff values observed in this series resulting in at least 10 patients in the groups were considered. The green shading indicates the cutoff used.

High MYO1A[1]	*Low MYO1A*[2]	*MYO1A IHC cutoff*[3]	*DFS Logrank p-value*[4]	*Mean DFS survival (high)*[5]	*Mean DFS survival (low)*[6]	*OS Logrank p-value*[4]	*Mean OS survival (high)*[8]	*Mean OS survival (low)*[9]
138	**17**	1.2	0.4292	3.1	1.5	0.6089	4.3	1.9
134	**21**	1.3	0.2566	3.6	1.0	0.4675	4.5	2.4
127	**28**	1.5	0.1964	3.7	1.5	0.2165	4.6	2.2
124	**31**	1.7	0.1801	3.7	1.0	0.1209	4.7	1.9
119	**36**	1.8	0.0632	3.7	1.0	0.1494	4.6	2.2
113	**42**	2.0	0.0311	3.8	1.0	0.0799	4.8	1.8
102	**53**	2.2	0.0172	6.2	1.0	0.0403	5.0	1.9
95	**60**	2.3	**0.0042**	>9	1.0	**0.0097**	5.5	1.8
86	**69**	2.5	0.0787	6.2	1.5	0.1009	5.0	2.5
75	**80**	2.7	0.6639	3.1	2.4	0.6607	4.8	3.5
70	**85**	2.8	0.6302	3.1	2.4	0.5990	4.8	3.1
55	**100**	3.0	0.2191	6.2	2.2	0.2088	5.3	2.9
42	**113**	3.2	0.4513	6.2	2.4	0.3591	5.1	3.4
35	**120**	3.3	0.5026	6.2	2.4	0.2268	6.2	3.6
25	**130**	3.5	0.3168	6.2	2.4	0.1837	6.2	3.6
17	**138**	3.7	0.4273	>9	2.5	0.2711	>9	4.0

[1]Number of patients in the high MYO1A group; [2]number of patients in the low MYO1A group; [3]average of triplicate replicates stained in the tissue microarray; [4]Logrank p-value of the comparison of the disease-free survival (DFS) of patients in the high and low MYO1A groups; [5]mean disease-free survival in the group of patients with high tumor MYO1A; [6]mean disease-free survival in the group of patients with low tumor MYO1A; [7]Logrank p-value of the comparison of the overall survival (OS) of patients in the high and low MYO1A groups; [8]mean overall survival in the group of patients with high tumor MYO1A; [9]Mean overall survival in the group of patients with low tumor MYO1A.

Supporting Table 5: Primers used for amplification of the coding *MYO1A* region, bisulfite sequencing and Real-Time RT-PCR.

Primer name	*Primers used for*	*Primer sequence*	*Product size (bp)*	*Annealing temp. (ºC)*
MYO1A-EX2-3-F	Sequencing	TTACTGGCCCCTAAAGCTGA	496	67
MYO1A-EX2-3-R	Sequencing	CTTCAGGGGAAGGGACAAAG		
MYO1A-EX4-5-F	Sequencing	GCCCAGTCTGCTCCAAGTAG	584	68
MYO1A-EX4-5-R	Sequencing	TGATTCTGGGGGTTAGATGG		
MYO1A-EX6-8-F	Sequencing	CCCTTCCTCCTTTCCCTTC	676	64
MYO1A-EX6-8-R	Sequencing	GAATGGAGGTTGGGGACTTT		
MYO1A-EX9-10-F	Sequencing	GTGAGGTGTCAAGGCTGGAG	500	68
MYO1A-EX9-10-R	Sequencing	GATGGTAGAAGGACACGACTTG		
MYO1A-EX11-12-F	Sequencing	ACTCCCTCCCCTGAGAGAAA	399	64
MYO1A-EX11-12-R	Sequencing	CAGGAAGGTGAGGCAGACAG		
MYO1A-EX13-14-F	Sequencing	TCTGTTTGCCCCCTACTCC	484	68
MYO1A-EX13-14-R	Sequencing	CAAGGAGAAAGGAAGCTCTGG		
MYO1A-EX15-16-F	Sequencing	TGAGGTCTCTGGAGGCTTGT	581	68
MYO1A-EX15-16-R	Sequencing	GACTTCAGTCTGGGCCTGAG		
MYO1A-EX17-F	Sequencing	GGGAAGGTGAGAGTCTGGAA	399	68
MYO1A-EX17-R	Sequencing	GTGTTCTACAGCGCATGGAC		
MYO1A-EX18-19-F	Sequencing	ACACTGGCAATGATGTCAGC	648	65
MYO1A-EX18-19-R	Sequencing	CAGCCTTTCTCAGGTGGGCT		
MYO1A-EX20-21-F	Sequencing	GGGGTATAGGAGAGGACAGCA	456	69
MYO1A-EX20-21-R	Sequencing	CTAGCCAGCAGGTGACACAA		
MYO1A-EX22-F	Sequencing	ACTCAGGTCTTTGCGTGGTT	244	67
MYO1A-EX22-R	Sequencing	GCCTCTTCTCAAACCCCTCT		
MYO1A-EX23-F	Sequencing	CCTTTGAAGTGGCAGGATCT	300	67
MYO1A-EX23-R	Sequencing	GGGAGGCAAAAGAGGAAAAT		
MYO1A-EX24-25-F	Sequencing	CTGTCCCTCCTTCCTCACAG	724	67
MYO1A-EX24-25-R	Sequencing	ACTAGCTGCGGGAGGAGTTC		
MYO1A-EX26-27-F	Sequencing	GAGTGGGGGCAATTAATCCT	594	67
MYO1A-EX26-27-R	Sequencing	TTCGCTTTCTGATCCTGGTC		
MYO1A-EX28-F	Sequencing	AGGGGATGGGCACTAGACTT	499	65
MYO1A-EX28-R	Sequencing	CAAGGAGCTTGAGGAGGAAA		
MYO1A-BISULF-CG154-F	Bisulfite seq.	TTTAAATTTGGGAGATAATGGAGTAAG	174	56
MYO1A-BISULF-CG154-R	Bisulfite seq.	AATCAACACAAAATCCAAACTATTC		
MYOIA-QPCR-F	qPCR	TTCCTACTGGGGCTGAAGAA	99	60
MYOIA-QPCR-R	qPCR	CTCCTGATTTGCTGTGCTGA		

Figure S1

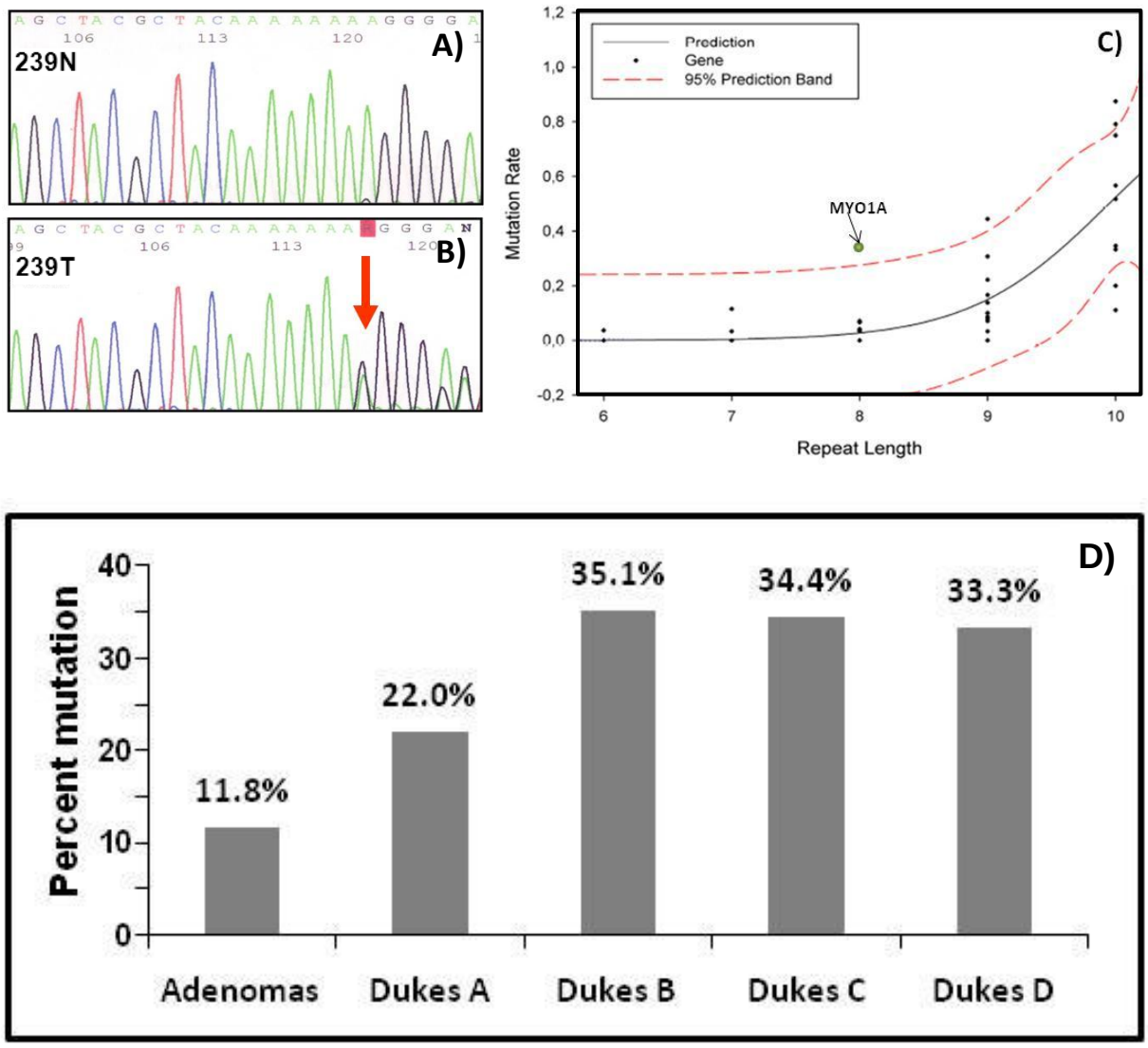

Figure S1: Frequent MYO1A frameshift mutations are found in MSI colorectal tumors. Panel A) shows the sequence of the MYO1A Exon 28 fragment containing the A8 tract in the normal tissue of a colon cancer patient. The heterozygous A8->A7 mutation in the tumor DNA of this patient is shown in panel B). C) Logistic regression model for the identification of real targets using 62 control intronic repeats as described (1). The solid black line denotes the regression prediction curve derived from the intronic control repeats (black symbols). The red dashed lines are the upper and lower limit of the 95% prediction interval that is derived using the standard errors and the asymptotic variances (1). MYO1A is shown as a green dot. D) Percentage of MYO1A mutations observed in MSI adenomas and carcinomas of different Dukes stage. Fisher's exact test in adenomas/Dukes A vs. Dukes B-D, p=0.04.

Figure S2

A

MYO1A

3091 aaa aaa aag ggg agt cat tgc ttg gag gtg act gtg cag tga

1030 K K K G S H C L E V T V Q

MYO1A^{7A}

3091 aaa aaa agg gga gtc att gct tgg agg tga

1030 K K R G V I A W R

B

Figure S2: Mutation effects on the MYO1A protein. A) DNA (upper lines) and protein (lower lines) sequences of the C-termini of MYO1A and MYO1A^{7A}. The 8A 3901-3908 to 7A mutation results in a replacement of the last 11 amino acids of MYO1A with 7 different amino acids. The basic (underline) and acidic (double underline) residues are indicated. B) Constructs used in this study. All proteins are fused to an N-terminal EGFP or ERFP. The numbers indicate the first and last amino acids of each protein.

Figure S3

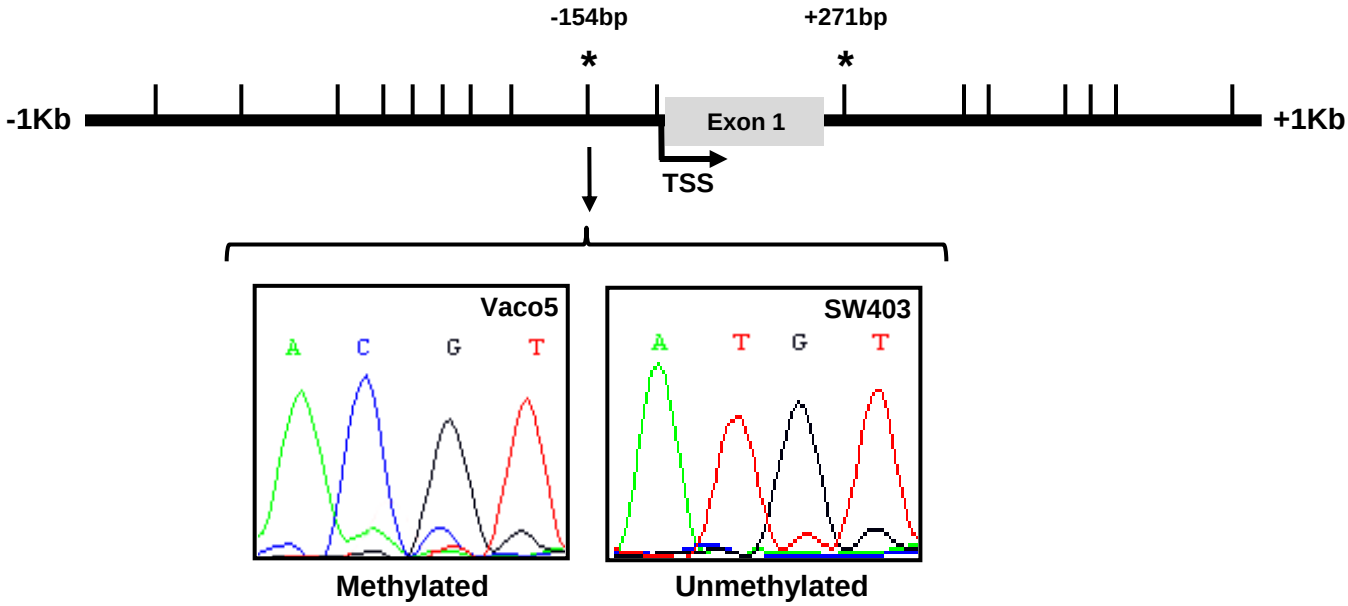

Figure S3: CpG dinucleotides in the *MYO1A* promoter. Location of CpG dinucleotides (vertical lines) in 2Kb around the transcription start site (TSS) of human MYO1A. The two CpGs investigated are indicated by asterisks (located at -154bp and +271bp relative to the TSS). Examples of the results of direct sequencing after bisulfite treatment are shown for cell lines with and without methylation.

Figure S4

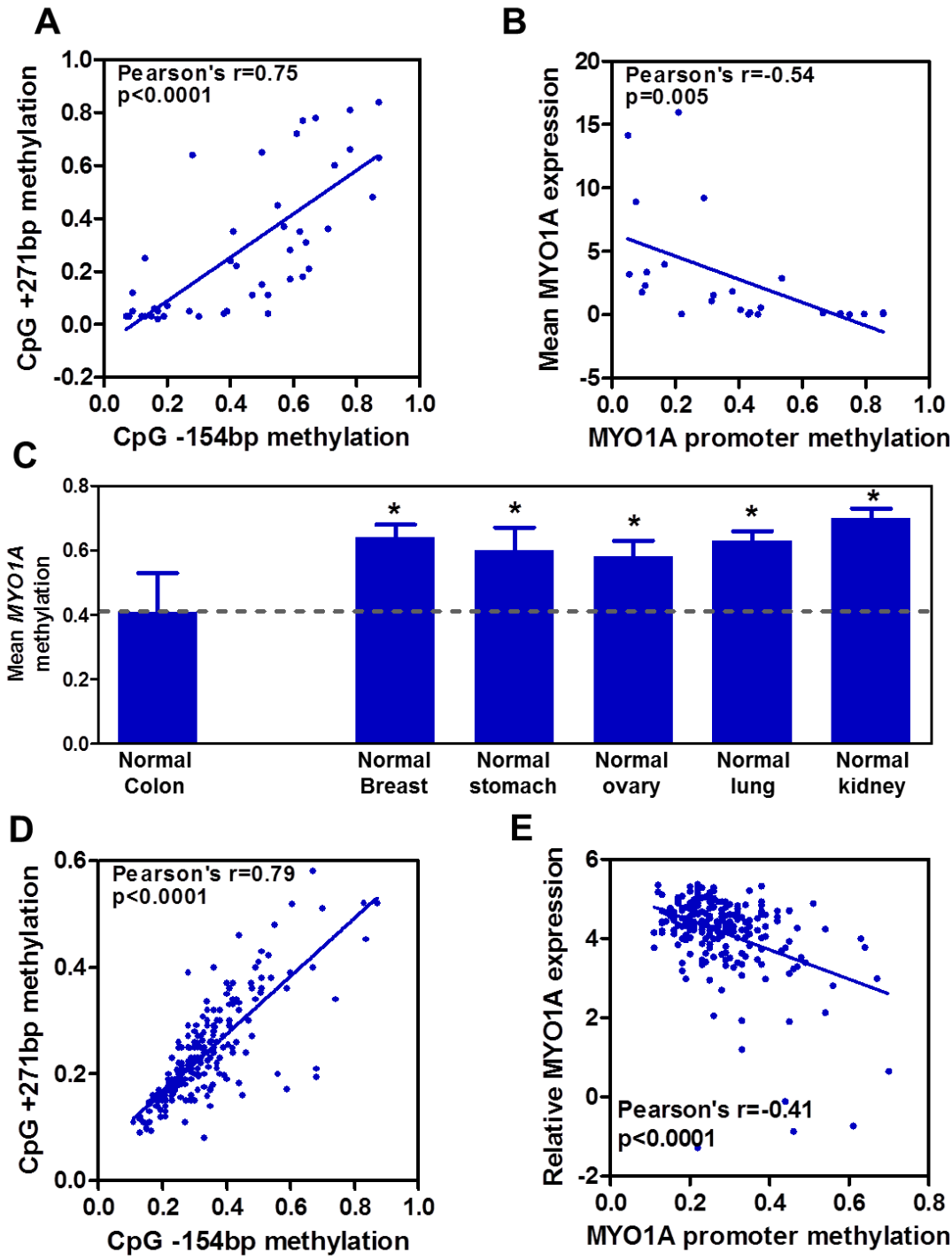

Figure S4: *MYO1A* promoter methylation and mRNA expression levels. A) Correlation between methylation levels of two CpGs in position -154bp and +271bp relative to the transcription start site of *MYO1A* in 46 colorectal cancer cell lines. B) Correlation between the mean methylation levels in the *MYO1A* promoter and MYO1A expression levels in colorectal cancer cell lines. C) Average levels of *MYO1A* promoter methylation in normal human tissues. Asterisk indicates $p<2.6x10^{-19}$. D) Correlation between the levels of methylation of the CpGs located in position -154bp and +271bp in a series of 222 primary colorectal tumors. E) Correlation between the mean methylation levels in the *MYO1A* promoter and MYO1A expression levels in 222 primary colorectal tumors.

Figure S5

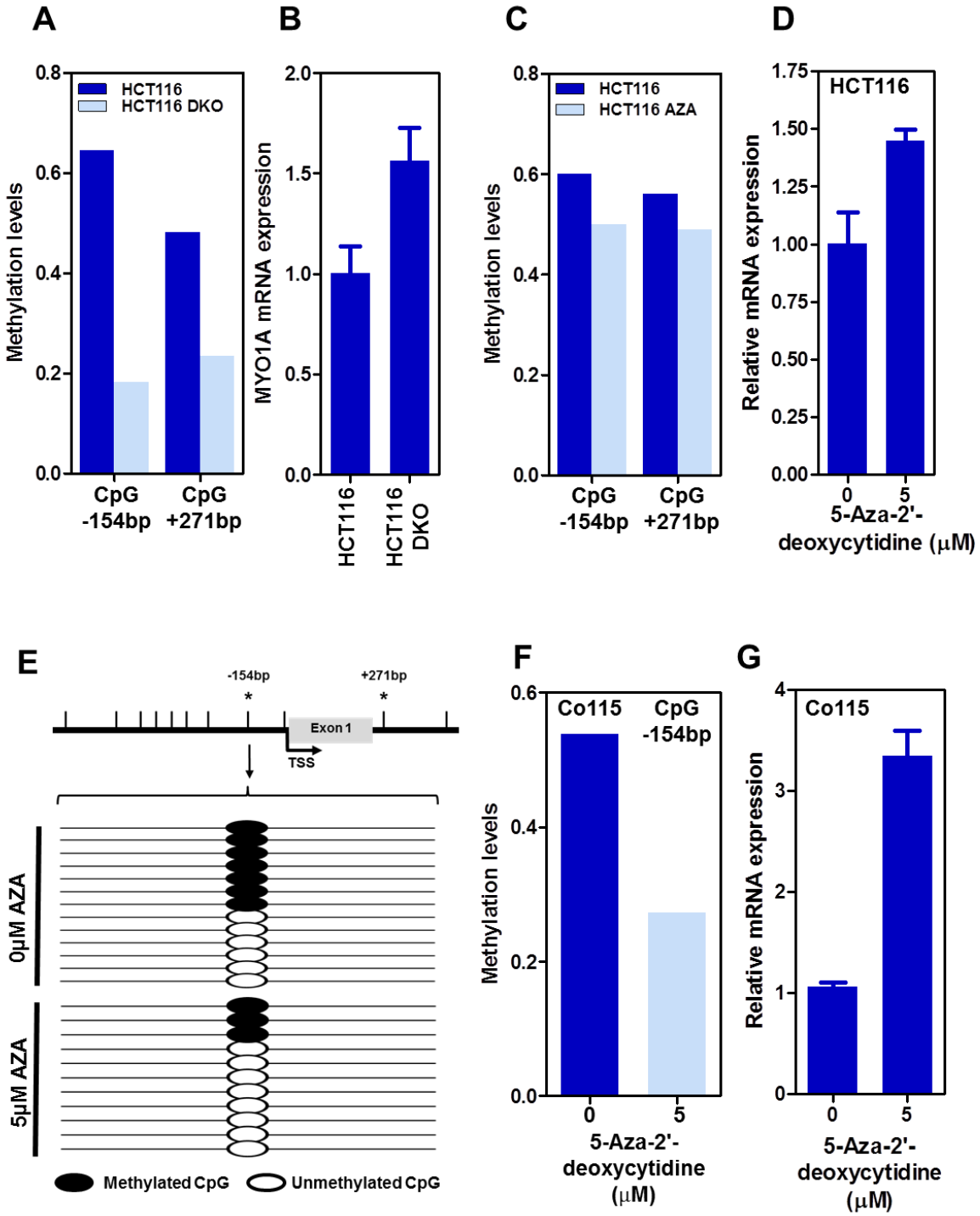

Figure S5: Methylation of the *MYO1A* promoter regulates gene expression. Inactivation of DNA methyltransferases in HCT116 colon cancer cells either A) genetically (DNMT1 and DNMT3b double KO –DKO; Gene Expression Omnibus GSE26990 (2)) or C) pharmacologically (5-aza-2'-deoxycytidine; ArrayExpress E-MTAB-210 (3)) resulted in reduced levels of MYO1A promoter methylation (CpGs located -154bp and +271bp relative to MYO1A transcription start site - TSS). This was associates with increased MYO1A mRNA levels as determined by quantitative Real-Time RT-PCR (B and D). Panels E) and F) show the proportion of alleles methylated and unmethylated after sequencing of PCR amplified promoter regions of bisulfite-converted Co115 DNA samples treated with the indicated concentrations of 5-Aza-2'-deoxycytidine. Panel G) shows relative mRNA levels (Real-Time RT-PCR) in Co115 cells treated with the indicated concentrations of 5-Aza-2'-deoxycytidine.

Figure S6

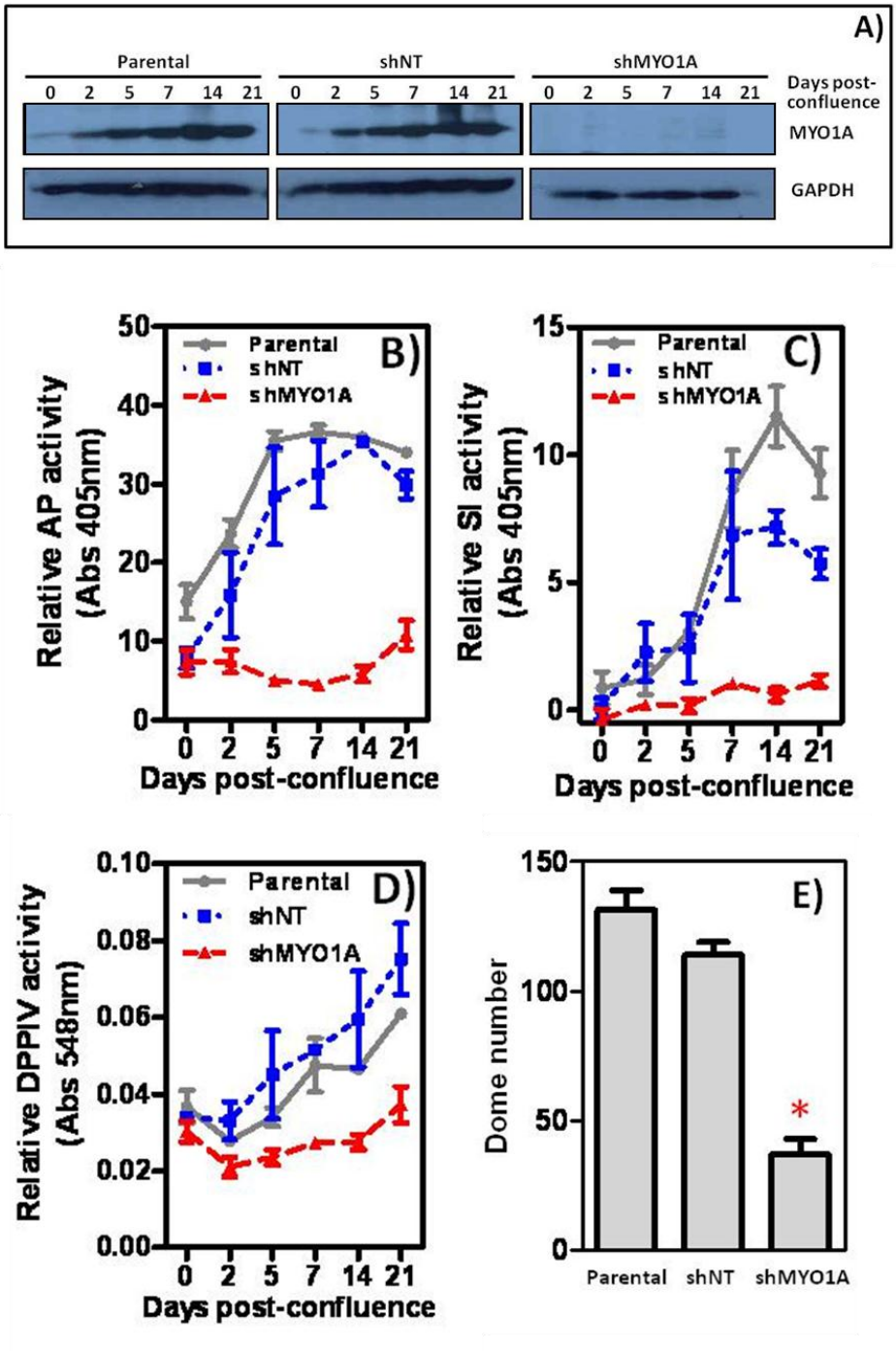

Figure S6: MYO1A regulates differentiation in colon cancer cells. Caco2BBe cells stably transduced with lentiviral particles carrying shMYO1A showed significantly reduced MYO1A expression during a 21-day timecourse in culture compared to parental cells and non-target shRNA (shNT) transduced cells (A). MYO1A knockdown resulted in a significant reduction of the activity of brush border enzymes such as alkaline phosphatase (B; Student's t-test at day 21 p=0.002), sucrose-isomaltase (C; Student's t-test at day 21 p=0.008) and dipeptidyl-peptidase IV (D; Student's t-test at day 21 p=0.007). Reduced MYO1A levels also resulted in a significant decrease in the number of domes observed in Caco-2 cells after three weeks in culture (E; Student's t-test p=0.01). Results shown are the mean ± SD of 3 independent experiments carried out in triplicate.

Figure S7

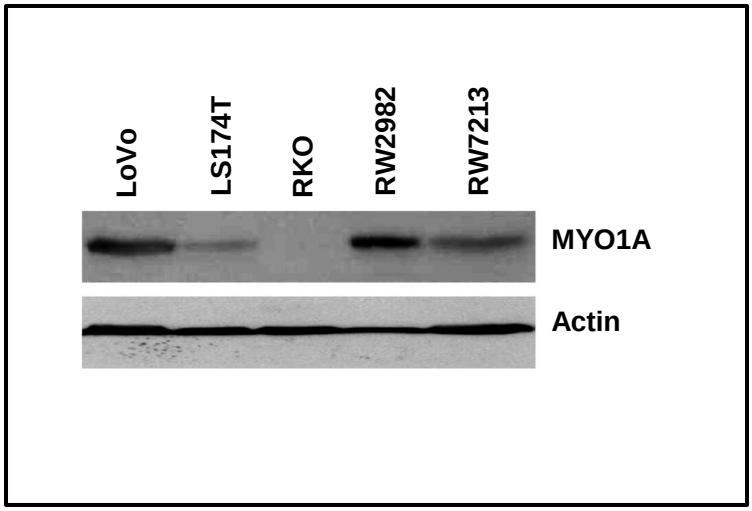

Figure S7: MYO1A protein levels in several colon cancer cell lines. The relative levels of MYO1A protein levels in different colon cancer cell lines growing exponentially was determined by Western blotting as described in the 'Experimental Procedures' section. Actin was used as a loading control.

Figure S8

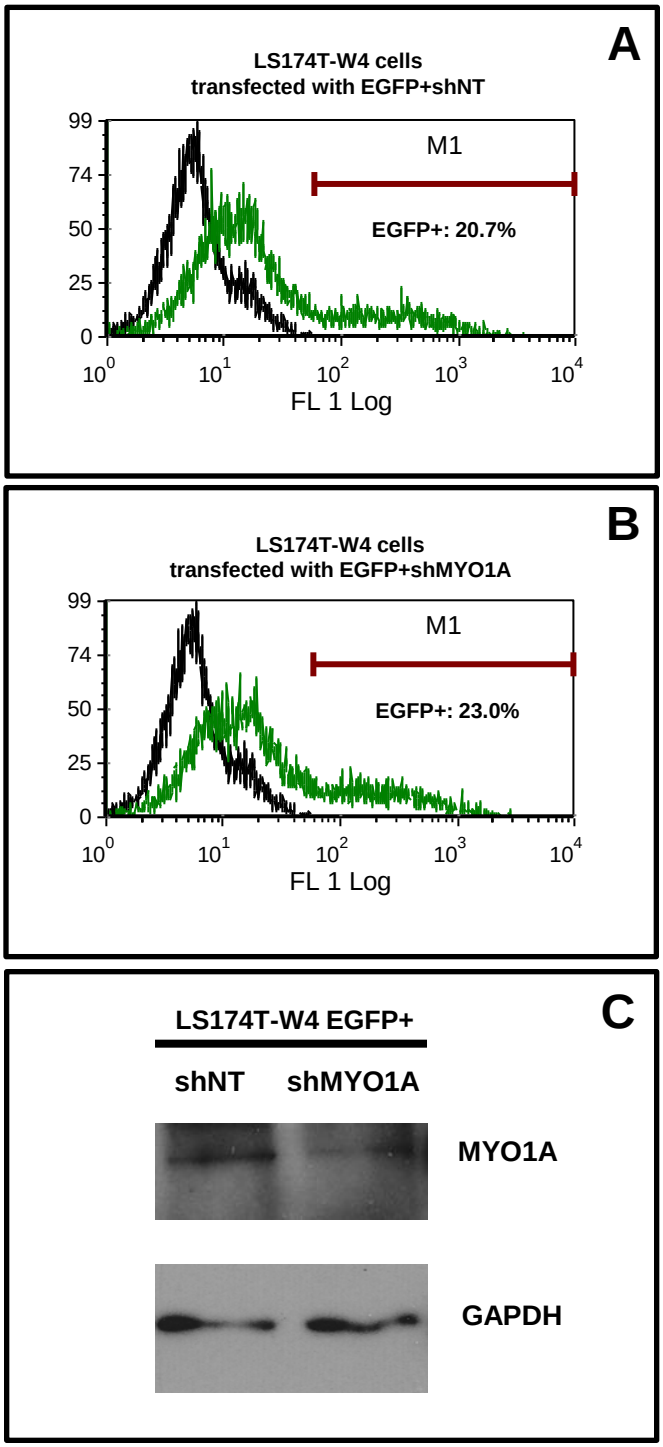

Figure S8: MYO1A knock down in LS174T cells. To assess the levels of MYO1A knock down achieved in the experiments with LS174T-W4 cells, EGFP was cotransfected with either control non-target shNT (A) or shMYO1A (B). After 48h, LKB1 overexpression was induced with doxycyclin (5μg/ml) and 24h later EGFP positive cells (M1 region; the percentage of EGFP positive cells is shown) were sorted using a FACSAria cell sorter (Becton, Dickinson) and used for assessment of MYO1A protein levels by Western blotting (C). Relative MYO1A levels were quantified by densitometry using GAPDH as a loading control. Numbers under the MYO1A band show the relative levels of MYO1A.

Figure S9

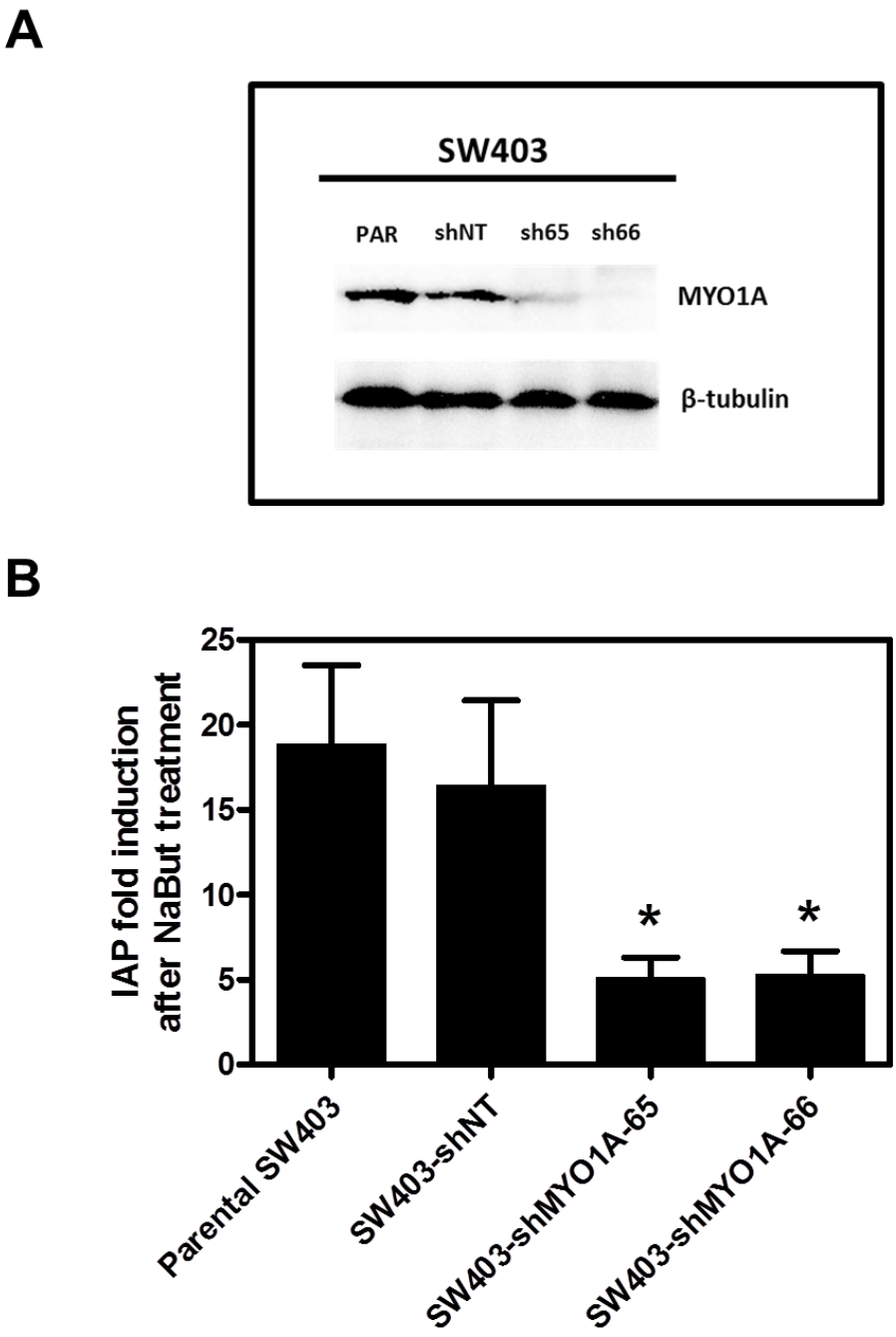

Figure S9: Reduced MYO1A levels interfered with butyrate-induced alkaline phosphatase activity in SW403 cells. A) Transduction of SW403 colon cancer cells with two different shRNAs against MYO1A (shMYO1A-65 and shMYO1A-66) resulted in significantly reduced levels of MYO1A protein (Western blotting). B) Butyrate treatment (5mM for 72h) of parental and non-target shRNA SW403 cells (shNT) resulted in a significant increase in the levels of intestinal alkaline phosphatase (IAP) activity, a marker of differentiation along the absorptive cell lineage. However, transduction of SW403 cell with two different shRNAs against MYO1A (shMYO1A-65 and shMYO1A-66) significantly reduced the butyrate-induced increase of IAP (Student's T-test $p<0.05$). Mean±SE of four independent experiments is shown.

Figure S10

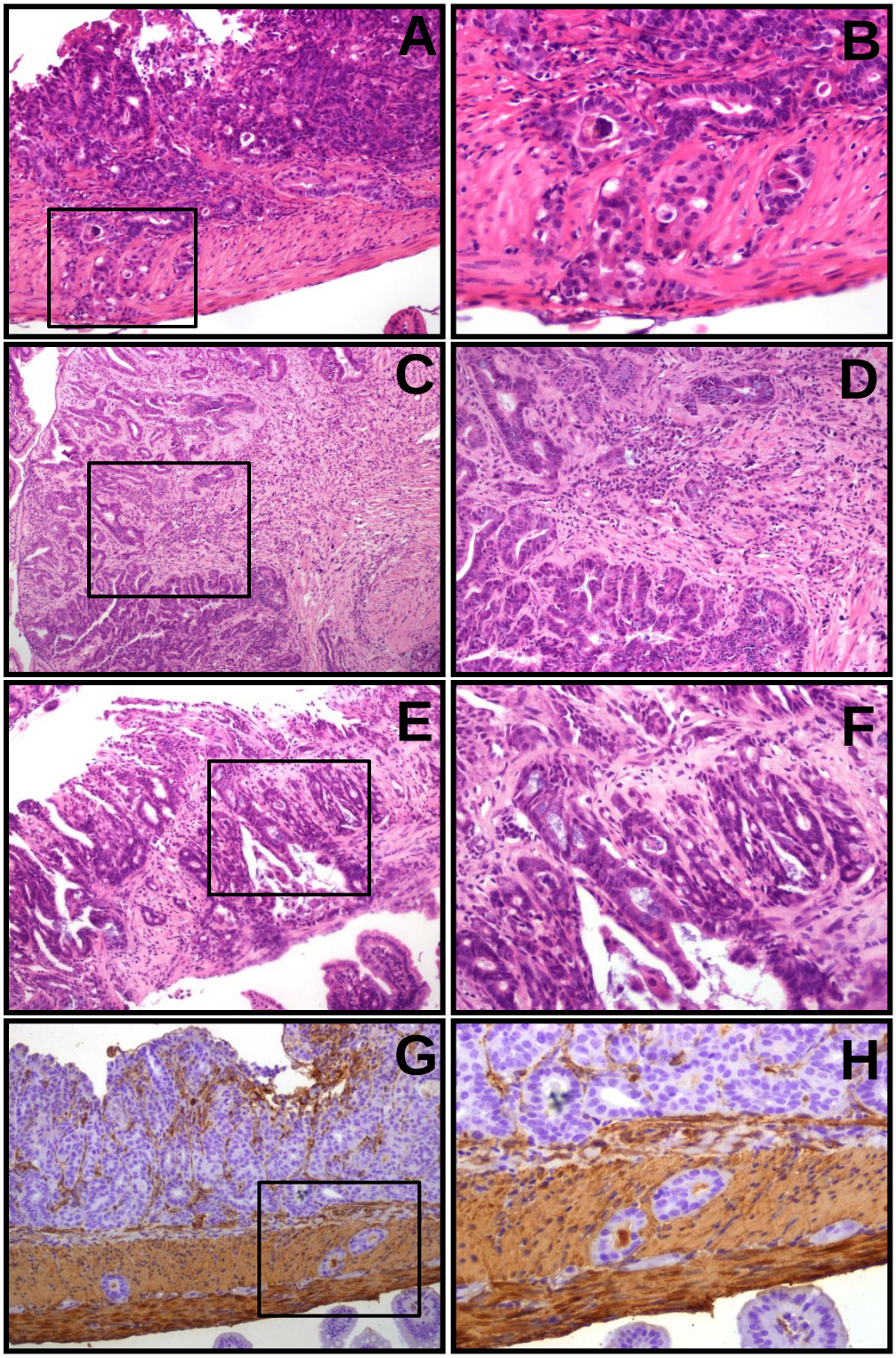

Figure S10: Histology of adenocarcinomas in the intestine of $Apc^{min/+}$;$Myo1a^{-/-}$ mice. Panels A, C and E show the histology of infiltrating adenocarcinomas in the small intestine of $Apc^{min/+}$;$Myo1a^{-/-}$ mice. Higher magnification of the indicated areas is shown in B, D and F. Panels G-H show immunohistochemical staining with alpha smooth muscle actin of an invading adenocarcinoma demonstrating tumor invasion through the muscle layers of the intestine.

Figure S11

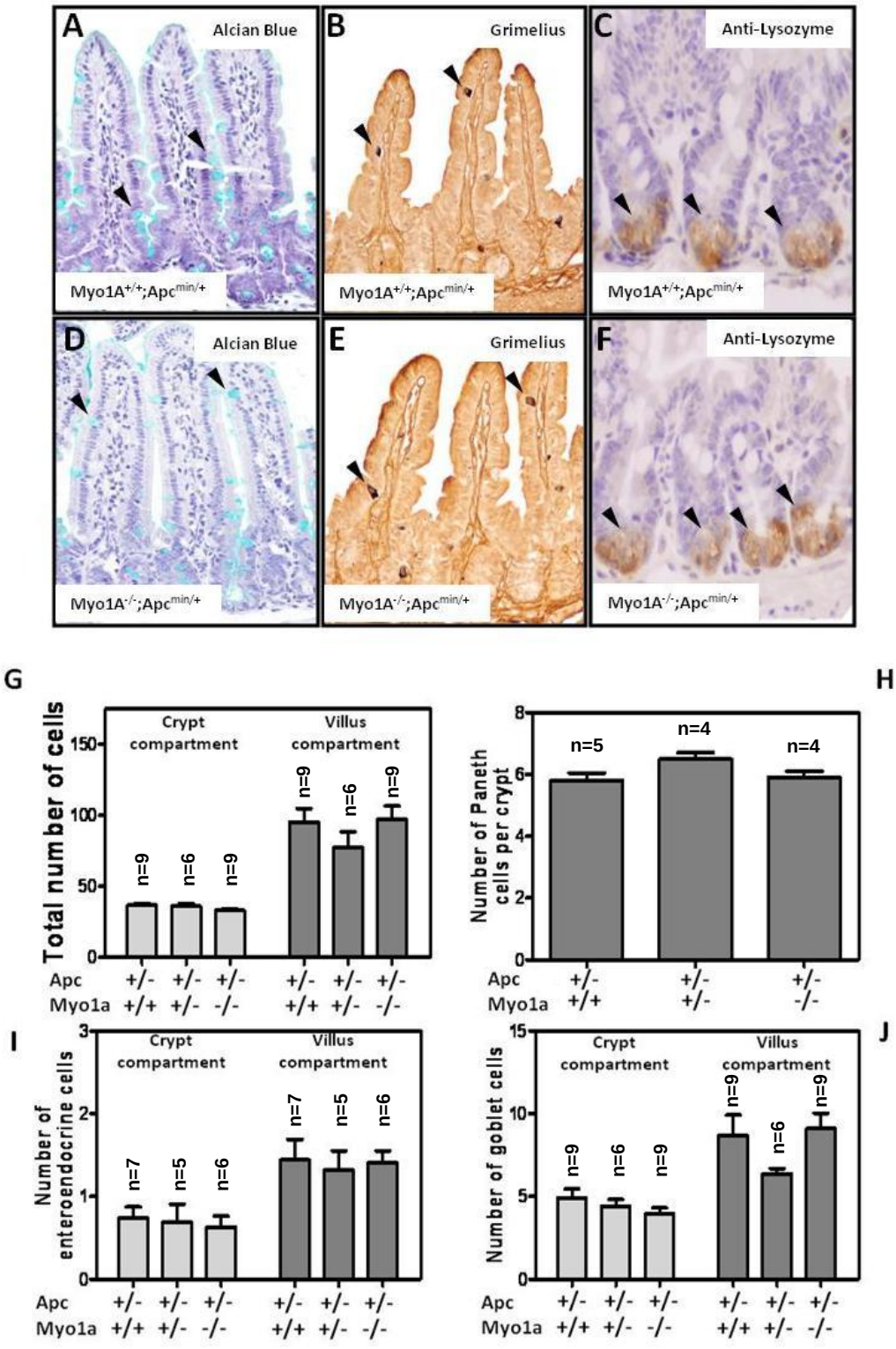

Figure S11: Effects of *Myo1a* inactivation in the number of intestinal epithelial cells. Goblet (A, D), enteroendocrine (B,E) and Paneth cells (C,F) were detected with 1% Alcian blue, Grimelius staining and anti-Lysozyme immunostaining, respectively. Arrow heads indicate the different epithelial cell types. $Apc^{Min/+}$ mice that are wild type, heterozygous or homozygous *Myo1a* mutants did not differ in the total number of cells (G), Paneth (H), enteroendocrine (I) or goblet cells (J). The number of animals studied is indicated above the bars in each histogram. Mean ± SE is shown.

Figure S12

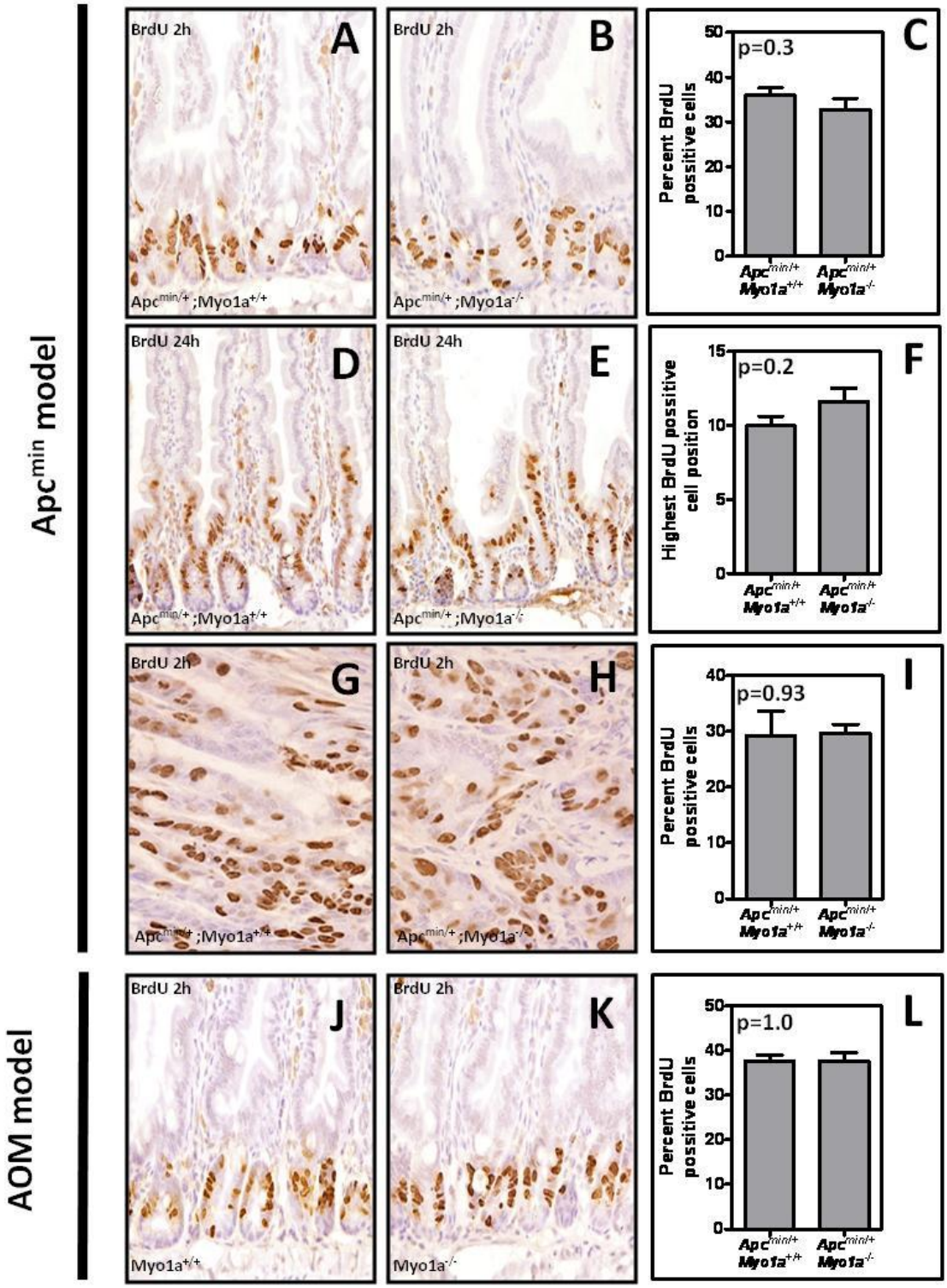

Figure S12: Proliferation and cell motility in the intestine of *Myo1a* knockout mice. Mice were i.p. injected with 100mg/Kg bromodeoxyuridine (BrdU) 2 or 24h before being sacrificed. The number of cells in S-phase of the cycle during this time was assessed by anti-BrdU immunohistochemistry. No differences in the number (A-C; 6 wild type and 8 KO mice) or location (D-F; 6 wild type and 6 KO mice) of BrdU-positive cells was observed in the normal epithelium (A-F) or the small intestinal tumors of $Apc^{min/+}$ mice (G-I) or AOM-treated animals (J-L; 8 wild type and 11 KO mice) that were either wild type or null for *Myo1a*. Mean ± SE is shown in the histograms.

Figure S13

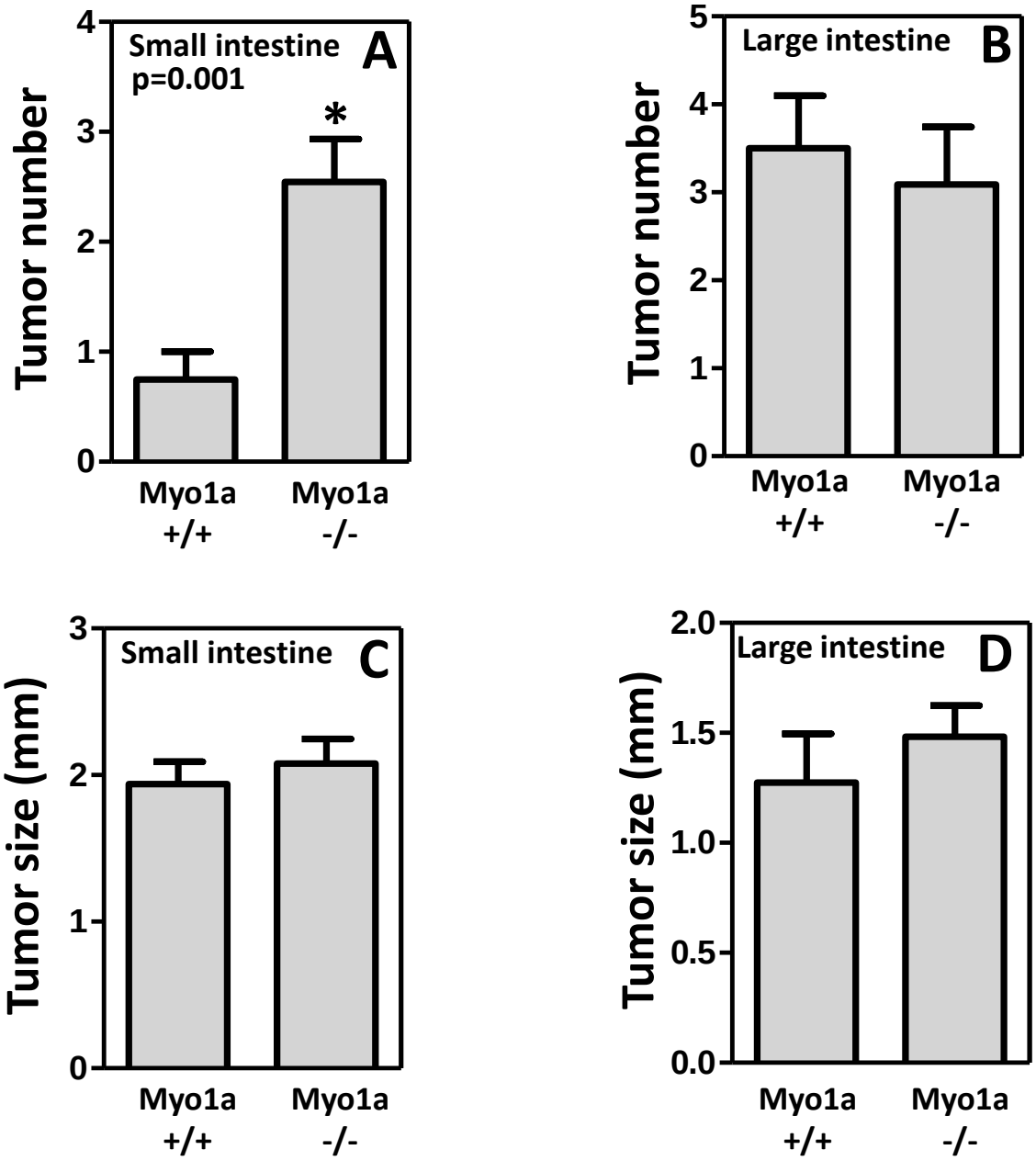

Figure S13: Size and number of AOM-induced tumors in *Myo1a* knockout mice. Animals received 6 weekly i.p. injections of 10mg/Kg azoxymethane (AOM) starting at nine weeks of age and were euthanized 10 weeks after the last injection. AOM treatment resulted in tumor formation in the small and large intestine. The vast majority of these tumors were adenomas with low grade dysplasia. Myo1a$^{-/-}$ mice (n=11) showed a significant increase (Student's t-test p=0.001) in the number of tumors in the small intestine (A), but not in the large intestine (B), compared to Myo1a$^{+/+}$ animals (n=8). C-D) No differences were observed in the size of the tumors found in the small and large intestine of Myo1a$^{+/+}$ and Myo1a$^{-/-}$ animals. Mean ± SE is shown.

Figure S14

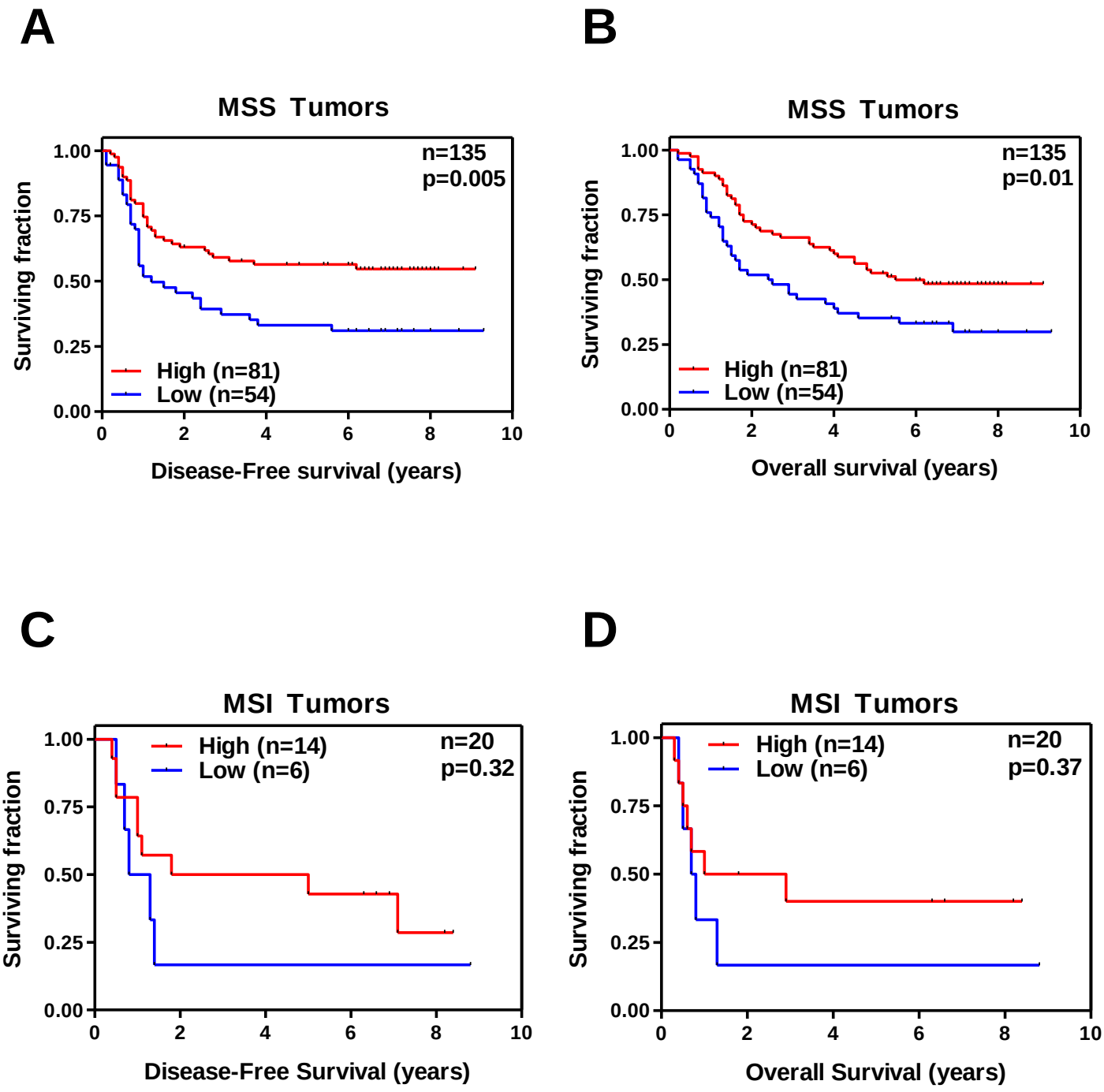

Figure S14: MYO1A and prognosis of colorectal cancer patients with MSS and MSI tumors. Colorectal cancer patients with MSS tumors that had low levels of MYO1A protein showed significantly shorter disease-free (A) and overall survival (B). A corresponding trend was also observed for shorter survival in colorectal cancer patients with MSI tumors with low MYO1A levels, although the differences did not reach statistical significance (C-D).